Asymptotically-correct modified strain gradient modelling of micro and nano beams

Renuka Sahu (Department of Aerospace Engineering, Indian Institute of Science, Bengaluru – 560 012, India. Email: renukasahu@iisc.ac.in) (https://orcid.org/0000-0002-1090-9475)

Dineshkumar Harursampath (Department of Aerospace Engineering, Indian Institute of Science, Bengaluru – 560 012, India. Email: dineshkumar@iisc.ac.in) (http://orcid.org/0000-0001-6855-303X)

J Ranjan Banerjee (Department of Engineering, City St George's, University of London, London- EC1V 0HB, United Kingdom. Email: j.r.banerjee@city.ac.uk) (https://orcid.org/0000-0002-5524-3742)

Sathiskumar A. Ponnusami* (Department of Engineering, City St George's, University of London, London- EC1V 0HB, United Kingdom. Email: sathiskumar.ponnusami@city.ac.uk) (https://orcid.org/0000-0002-2143-8971)

Abstract- This paper introduces a novel approach to model length-scale effects in micro and nano beams with square and rectangular cross sections by using the dimensional reduction technique and variational asymptotic method (VAM). Traditional continuum approaches have been advanced by accounting for the length-scale effects, which have gained significant importance in micro- and nano-scale applications like MEMS and NEMS devices, in recent years. In this context, an asymptotically-correct modified strain gradient beam theory has been developed by incorporating higher-order length-scale parameters through VAM, integrating the strain gradient theory within the VAM framework for the first time. The formulation is focused on rectangular and square cross section beams, whereby an originally three-dimensional structure is reduced to an energy equivalent one-dimensional beam using the modified strain gradient theory as the underlying constitutive behaviour. A systematic investigation has been conducted to assess the effect of the choice of the order of the material length-scale parameter, providing considerable insights into the appropriateness of the choice regarding the beam behaviour. It is shown that choosing the order of the length-scale parameter as O (l)=O (b) is the most appropriate, where l is the material length-scale parameter and b is the width of the beam. Other two possible choices, O (l)=O (L), L being the beam length and O (l)<<O (b) are shown to be inconsistent because the former ignores the classical strain energy contributions whereas the latter ignores the strain-gradient terms. Hence, using O (l)=O (b), the zeroth- and the first-order strain gradient beam theories have been derived based on the VAM-based dimensional reduction procedure. The results are compared with those available in the literature. The developed theory captures the stiffening effect of the length-scale parameters and establishes an asymptotically-accurate beam model that includes higher strain gradient effects. The proposed beam theory is applied to Carbon Nano Tube (CNT)-reinforced composite micro beams, to investigate the length-scale-dependent behaviour of the micro beams when subjected to bending loads.

Keywords: Strain Gradient Theory, Variational Asymptotic Method, Micro- beam, Analytical model, Length-scale parameter, Carbon nano tube

1. Introduction

Traditionally, continuum elasticity models are based on the approximation of locality, meaning that the stress at a point in the material depends only on the strain at that point. This approximation holds quite well for the macroscale structures, where small-scale effects are not so predominant. However, as micro- and nano-scale devices are increasingly becoming useful and popular, it is important to include small-scale parameters to predict accurately the

mechanical behaviour of such structures [1-3]. Thus, various theories, such as the non-local elasticity [4] and higher-order continuum [5] theories, have been developed. In particular, the couple stress theory and the strain gradient theory, combine the macroscopic deformation of materials with the internal microstructure of the material by incorporating higher-order spatial gradients of the displacement field. These higher-order continuum theories provide more accurate and refined models for the mechanical behaviour of materials than traditional continuum mechanics and therefore, are important in the design and analysis of micro- and nano-scale devices, where the device's size is comparable to the size of the material's microstructure [6-9].

In 1963, Mindlin presented the couple stress theory [10], which models the behaviour of a linear three-dimensional elastic continuum by incorporating the microstructural deformational behaviour. This classical couple stress theory was further developed by Toupin [11] and Koiter [12] containing four size parameters. In recent years, a modified couple stress theory has also been proposed which contains only one size parameter [13]. Experimental observations of micro beams also led to the conclusion of the size dependence of the beam stiffness and deflections. The strain gradient theory is another higher-order theory that considers the gradient of strain along with the traditional elastic strain as the deformation metric. The strain gradient theory differs from the couple stress theory (which is the earlier of the two) as it includes the rotation, dilatation, and deviatoric stretch gradients, whereas the couple stress theory includes only the rotation gradient. Lam et al. [14] observed that the dimensionless bending stiffness of an epoxy polymeric beam with a thickness of 20 μm was approximately 2.3 times higher than that of the beam with 115 μm thickness, demonstrating the impact of small size effect on the structural behaviour. The development of the modified strain gradient theory took place subsequently. Mindlin and Eshel proposed the general strain gradient theory [15], which has since been modified by Lam et al. [14] and termed as the modified strain gradient theory. Zhou et al. [16] presented another modification of Mindlin's general strain gradient theory by introducing two different orthogonal decompositions of the strain gradient tensor. They established three independent higher-order elastic constants, as opposed to the initial five independent higher-order elastic constants given by the general strain gradient theory for isotropic materials. Khorshidi [17] demonstrated that the material length-scale parameters used in these higher-order theories, like the modified couple stress theory, are not material constants, but depend on the material and geometry of the structures, meaning that their values are never fixed and are always changing in various dimensions. They also showed that both material hardening and softening behaviour can be captured using these theories.

As evident from the literature, the strain gradient theory and its modified versions have been used to investigate the bending, buckling, vibration behaviour, and plasticity of various micro- and nano structures, particularly beams [18-22], plates and thin shells [23, 24]. For instance, Kong et al. [25] applied strain gradient theory to Euler-Bernoulli beams and studied their bending and vibrational behaviour. It was noted that considering the higher-order size parameters led to an increase in the stiffness of the beam compared to the classical Euler-Bernoulli theory results. Additionally, due to the presence of these parameters, the natural frequency of the beam also increases when compared to that obtained by classical theories. Li et al. [26] applied the strain gradient theory for the bending problem of plane-strain beams and analysed the size effect as well as the Poisson's ratio effect on the bending behaviour. They observed a dominant effect of the material length-scale parameter corresponding to the dilatation gradient on the stiffening of the beam. By contrast, Ashoori and Mahmoodi [27] derived the modified strain gradient model and the couple stress model in general curvilinear coordinates.

Akgöz et al. [28] used the modified couple stress theory and strain gradient elasticity approach to examine the buckling behaviour of micro beams. They found that the critical buckling load obtained by the strain gradient theory was three times higher than the load obtained by using the modified couple stress theory. Zhang et al. [29] applied modified strain gradient elasticity to a non-classical Timoshenko beam element and studied the buckling and vibration characteristics. Asghari et al. [30] developed a Timoshenko theory-based strain gradient formulation to capture the geometrically nonlinear behaviour of micro beams undergoing large deflections. They considered an important practical case which is that of the hinged-hinged boundary conditions and observed that the nonlinear strain gradient beam model predicted the highest stiffness. In addition, it was shown that between the modified coupled stress beam model and the strain gradient theory-based beam model, the strain gradient theory model provides higher stiffness. Using Galerkin's method, Kahrobaiyan et al. [31] developed an FEM beam element based on the strain gradient theory. Like all other studies based on the strain gradient theory, they also concluded that for smaller beam thickness-to-length ratios, there is a large difference in the classical and non-classical stiffness results, which, however, reduces to classical stiffness results when this ratio increases significantly. Amiot [32] developed optimal constitutive equations for first and second-strain gradient elasticity, considering static admissibility conditions. The challenge to satisfy simultaneously all requirements for higher-grade elastic beam formulation was emphasized. It was suggested that optimal equations suitable for such beam formulation can be derived by relaxing constraints. However, the disparity between constitutive equations and static admissibility conditions must be minimised to achieve sufficiently accurate results. This type of formulation approaches conventional beam equations under Cauchy elasticity when the beam dimensions are necessarily large. Lazopoulos and Lazopoulos [33] studied the bending and buckling of thin strain-gradient beams, whilst indicating the importance of cross-sectional area when considering the bending of thin beams.

Further, dell'Isola and Misra [34] advocated the shift to adoption of principle of virtual work and variational methods as the fundamental postulates to mechanics and for developing higher order theories. Their work highlights that creation of metamaterials by realising different properties can be achieved by going beyond the paradigm of classical (Cauchy) continuum mechanics by involving positive definite strain energies, thus promoting generalized continuum theories particularly higher-gradient and higher-order continua. Aminpour and Rizzi [35] developed one dimensional direct continuum representation of CNT with microstructure and employing hyperelastic models with an internal scalar field representing cross-sectional deformation. Their formulation emerges from a unified variational perspective and aim to capture size-dependent nonlinear phenomena—necking, kinking, or stiffness variation—by enriching the kinematics beyond classical beam theory. In another work by the above-mentioned authors, a 1-D continuum model with internal structure derived from the micro mechanics of carbon nanosheet using the representative elementary volume (REV) was investigated. This REV defined the strain measures and was used to obtain strain energy density and develop a constitutive relation. Their work related the micro strain measures to continuum measures and are more concise in application to CNTs and nanosheets [36].

The classical strain gradient elasticity proposed by Lam et al. [14] serves as a seminal reference for higher-order continuum modelling; however, its simplifications—particularly the assumption of vanishing characteristic lengths—limit its regularization efficiency and physical interpretability. Recent developments in granular micromechanics offer more physically grounded routes to parameter identification. For instance, Barchiesi et al. [37]

and Misra et al. [38] derived isotropic strain gradient and micromorphic continua directly from granular assemblies, ensuring micro–macro consistency under geometrically nonlinear deformations. These approaches were further extended to elasto-plastic-damage solids [39] and granular concrete systems [40], demonstrating their versatility. Also, mixed finite element regularization proposed by Riesselmann et al. [41] provide computational parallels to the present analytical formulation, both contributing to the broader goal of robust higher-order continuum modelling. Complementary to these micromechanical frameworks, the present study focuses on employing the Variational Asymptotic Method (VAM) to derive a modified strain-gradient beam model through systematic dimensional reduction of three-dimensional elasticity. While the micromechanical formulations primarily focus on constitutive parameter identification, the VAM-based framework emphasizes asymptotic consistency and scale separation in slender structures.

The current paper presents a novel approach to formulate an asymptotically-correct strain gradient continuum beam theory by incorporating higher-order non-classical formulation into the classical linear kinematics through the application of VAM. The work presented here is the first of its kind particularly, in the context of VAM literature which until now focused on classical dimensionally-reduced order models for structural and material problems without considering any length-scale effects. In terms of the layout, the paper is divided into five sections. Following this Section 1 on Introduction, Section 2 briefly introduces the strain gradient theory and VAM in general. Then, Section 3 explains the methodology used in this study and the implementation of the new theory. Next, Section 4 presents the findings of the research together with some comparative results from the literature, followed by Section 5 with concluding remarks and scope for further research.

2. Preliminaries

2.1. Strain Gradient Theory

From the strain gradient theory, it is known that the strain energy of any material is not only dependent on the stress and strain but also on the higher order derivatives of the strain [42]. The associated non-local elasticity theory originates from the idea that the state of stress at a point in a continuum is not only dependent on the strains/ displacements at that location but also on the strains/displacements at the other neighbouring locations. In this way, the strain gradient theory describes the strain energy expression, as follows [42]:

$$W = W(\varepsilon_1, \varepsilon_2, \varepsilon_3) \tag{1}$$

with, $\varepsilon_1 = \varepsilon = \frac{1}{2}(\nabla u + u\nabla)$, $\varepsilon_2 = \nabla\nabla u$, $\varepsilon_3 = \nabla\nabla\nabla u$

where, W is the potential or strain energy density, u represents the displacement, ε_1 is the classical strain definition and $\varepsilon_2, \varepsilon_3$ give the gradients of the strain.

In this work, modified strain gradient formulation is used, which is basically an extension of Mindlin's theory used by Lam et al. [14]. This choice was driven by its suitability for the VAM framework for development of such non classical models, the first combination in the literature to the best of author's knowledge. The mathematical formulations developed in their work allow for a more seamless integration into the VAM framework, facilitating the efficient reduction of higher-dimensional problems into lower-dimensional beam models while incorporating strain gradient effects. Also, dell'Isola and Misra [34] have also made a strong case for the sue of variational

approaches to establish relation between micro and macro-balance laws, thereby supporting formulations based on strain energy and principle of virtual work. According to the modified strain gradient theory, for an isotropic material, the strain energy density (U) of a deformable material occupying a region in space is given as:

$$U = \frac{1}{2}\int \left(\sigma_{ij}\varepsilon_{ij} + p_i\gamma_i + \tau^{(1)}_{ijk}\eta^{(1)}_{ijk} + m^s_{ij}X^s_{ij}\right) \tag{2}$$

where,

$$\varepsilon_{ij} = \frac{1}{2}\left(\partial_i u_j + \partial_j u_i\right) \tag{3}$$

$$\gamma_i = \varepsilon_{mm,i} = \partial_i \varepsilon_{mm} \tag{4}$$

$$\eta^{(1)}_{ijk} = \frac{1}{3}\left(\partial_i\varepsilon_{jk} + \partial_j\varepsilon_{ki} + \partial_k\varepsilon_{ij}\right) - \frac{1}{15}\delta_{ij}(\partial_k\varepsilon_{mm} + 2\partial_m\varepsilon_{mk}) - \frac{1}{15}[\delta_{jk}(\partial_i\varepsilon_{mm} + 2\partial_m\varepsilon_{mi}) + \delta_{ki}\left(\partial_j\varepsilon_{mm} + 2\partial_m\varepsilon_{mj}\right)] \tag{5}$$

$$X^s_{ij} = \frac{1}{2}\left(e_{ipq}\partial_p\varepsilon_{qj} + e_{jpq}\partial_p\varepsilon_{qi}\right) \tag{6}$$

where ∂_i is the differential operator, u_i is the displacement vector, ε_{ij} is the strain tensor, $\varepsilon_{mm,i}$ is the dilatation gradient vector, $\eta^{(1)}_{ijk}$ is the deviatoric stretch gradient tensor, X^s_{ij} is the symmetric rotation gradient tensor, δ_{ij} and e_{ijk} are the Kronecker delta and the permutation tensor, respectively. (In the above and, also in subsequent equations, the index notation will be used with repeated indices denoting that the summation is extended from 1 to 3). The corresponding stress measures are given as:

$$\sigma_{ij} = K\,\delta_{ij}\varepsilon_{mm} + 2\mu\varepsilon'_{ij} \tag{7}$$

$$p_i = 2\mu l_o^2\gamma_i \tag{8}$$

$$\tau^{(1)}_{ijk} = 2\mu l_1^2\eta^{(1)}_{ijk} \tag{9}$$

$$m^s_{ij} = 2\mu l_2^2 X^s_{ij} \tag{10}$$

where, K is the bulk modulus, μ is the shear modulus and l_o, l_1, l_2 are the material length-scale parameters corresponding to the dilatation gradients, deviatoric stretch gradients and rotation gradients, respectively.

2.2. Variational Asymptotic Method (VAM)

VAM is a mathematical tool for dimensional reduction based on the combination of asymptotic and variational principles. It uses small parameters inherently present in any particular problem formulation to conduct dimensional reduction of an originally three-dimensional (3-D) problem to either a shell or plate (2-D) or to a beam (1-D) problem. Because of its inherent nature of not making any *ad hoc* assumptions in the kinematics, the VAM-based approach yields asymptotically-accurate reduced order models while providing excellent computational efficiency. A summary of VAM-based beam analysis is shown by a flow chart in Fig.1. Starting with the 3-D strain energy functional of the problem with geometrically-exact beam kinematics, the problem is split into a 2-D cross-sectional analysis yielding the beam stiffness matrix and a 1-D analysis to obtain ultimately the complete deformation field of the beam structure for any given boundary conditions.

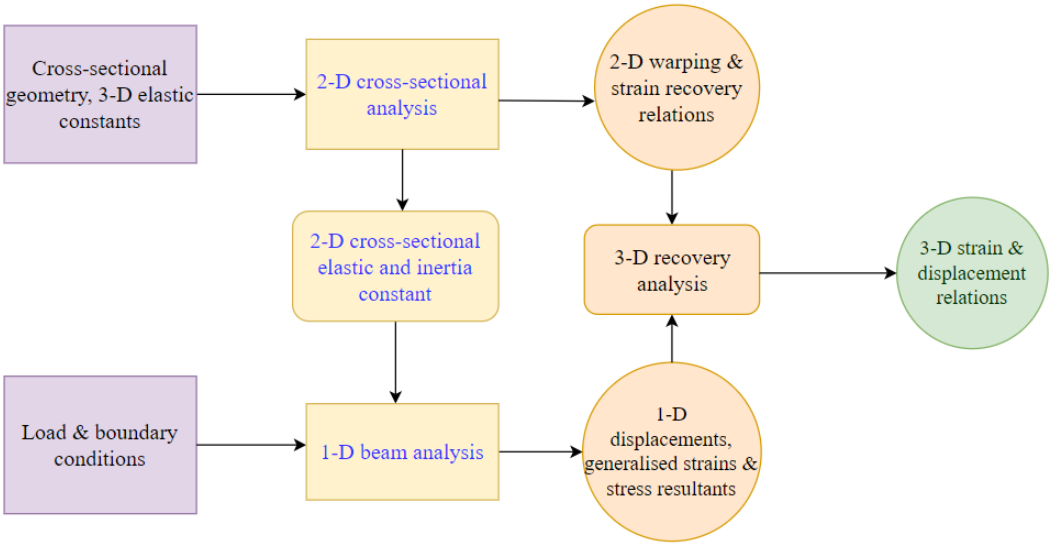

Fig.1. Flowchart representing the steps of beam analysis using VAM

In the following sections, the kinematic relations for a beam are derived, obtaining the zeroth-order approximations for the beam warping field, together with 1-D displacements and rotations. The strain-gradient terms are not considered here in this section for the sake of clarity, which will be dealt with, separately in Section 4. More details about the general approach of VAM can be found elsewhere [43-48].

2.2.1. *Kinematic Relations*

The slender beam structure, under consideration is represented by a reference line as shown in Fig.2. The reference cross section is taken to be normal to the reference line. The cartesian measures represented by x_1 and x_α where, ($\alpha = 2,3$) give the measure of reference line and cross section, respectively. The unit vectors for the coordinate systems for undeformed and deformed configurations are given by fixed dextral triads $\mathbf{b}_i$ and $\mathbf{B}_i$ respectively which are in two arbitrary frames b and B respectively (see Fig.2.).

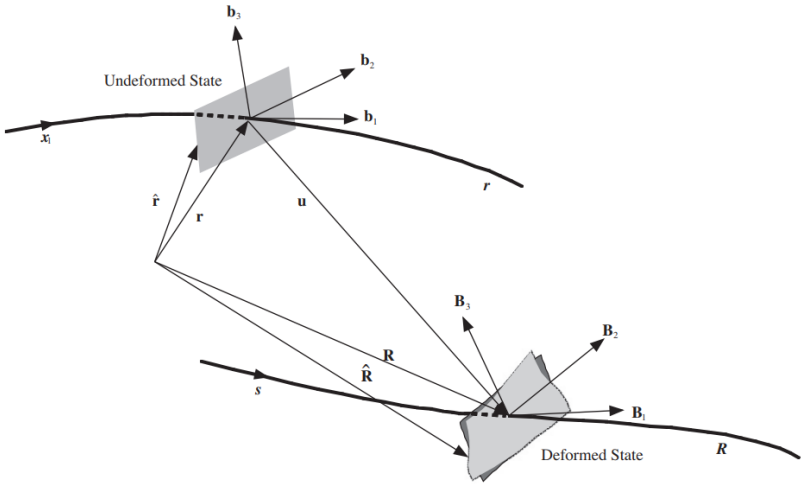

Fig.2. Schematic representing undeformed and deformed configuration with respective to coordinate systems

The relationship between the deformed and undeformed beam configurations, is represented by using the position vectors, $\hat{\mathbf{r}}$ in the undeformed configuration and $\widehat{\mathbf{R}}$ in the deformed configuration [43], as shown below.

$$\hat{\mathbf{r}}(x_1, x_2, x_3) = \mathbf{r}(x_1) + x_\alpha \mathbf{b}_\alpha \tag{11}$$

$$\widehat{\mathbf{R}}(x_1, x_2, x_3) = \mathbf{R}(x_1) + x_\alpha \mathbf{B}_\alpha(x_1) + w_i(x_1, x_2, x_3)\mathbf{B}_i(x_1) \tag{12}$$

where w_i represents the components of the warping function, i.e. w_1, w_2 and w_3 (both out of the cross-sectional plane and in-plane components respectively). These warping functions help to account for all possible deformations, i.e. out of plane deformations of the reference cross section which will be along the x_3 direction and in-plane deformations which will be along the x_1 or x_2 directions.
Using the above definition of the reference and deformed coordinates and configurations, the deformation gradient tensor (D_{ij}) is defined as follows:

$$D_{ij} = \mathbf{B}_i \cdot \mathbf{G}_k \mathbf{g}^k \cdot \mathbf{b}_j \tag{13}$$

and

$$\mathbf{G}_k = \frac{\partial \widehat{\mathbf{R}}}{\partial x_k} \tag{14}$$

$$\mathbf{g}^k = \mathbf{b}_k \tag{15}$$

Here, $\mathbf{G}_k$ are the covariant base vectors in the deformed configuration and $\mathbf{g}^k$ are the contravariant base vectors in the undeformed configuration. The 3-D linearised strain measures expressed in the undeformed basis are given as follows:

$$\Gamma_{ij} = \frac{1}{2}(D_{ij} + D_{ji}) - \delta_{ij} \tag{16}$$

where, δ_{ij} is the Kronecker delta function. Further, upon taking the small strain assumption, it can be shown that, by neglecting the products of warping and generalised 1-D strain terms (which are-γ_{11} is the 1-D extensional strain, κ_1 is the elastic twist rate and κ_2, κ_3 represent the bending curvatures) the simplified 3-D strain expressions are:

$$\Gamma_{11} = \gamma_{11} + x_3\kappa_2 - x_2\kappa_3 + w_1{}' \tag{17}$$
$$\Gamma_{22} = w_{2,2} \tag{18}$$
$$\Gamma_{33} = w_{3,3} \tag{19}$$
$$\Gamma_{12} = \frac{1}{2}(w_{1,2} - x_3\kappa_1 + w_2') \tag{20}$$
$$\Gamma_{13} = \frac{1}{2}(w_{1,3} + x_2\kappa_1 + w_3') \tag{21}$$
$$\Gamma_{23} = \frac{1}{2}(w_{3,2} + w_{2,3}) \tag{22}$$

Here, and throughout the paper, the superscript $(\_)'$ denotes derivative with respect to x_1, whereas the subscripts $(\_)_{,2}$ and $(\_)_{,3}$ denote derivatives with respect to x_2 and x_3 respectively.

2.2.2. Order Analysis and Warping Solutions

VAM is rooted in its foundations based on the procedure of order analysis. It is at this step where the asymptotic part of the analysis comes into play. Relying on the principles of calculus of variations, the strain energy density functional of a beam in terms of the kinematical parameters and unknown warping and asymptotically segregated terms in terms of their orders, are identified. The classical strain energy density of the beam (strain energy per unit length of the beam or strain energy of the cross section) is given as follows:

$$U = \frac{1}{2}\langle\langle E_{ijkl}\Gamma_{ij}\Gamma_{kl}\rangle\rangle \tag{23}$$

Here, $\langle\langle . \rangle\rangle$ denotes the integration over the cross section given as $\langle\langle . \rangle\rangle = \oint(.) g_0\, dx_2 dx_3$ and E_{ijkl} is the 3-D material stiffness matrix. g_0 is the determinant of the metric tensor for the undeformed state and is defined as $\sqrt{\det(\boldsymbol{g}_i \cdot \boldsymbol{g}_j)}$. Here, $\boldsymbol{g}_i$ and $\boldsymbol{g}_j$ represent the covariant base vectors in the undeformed configuration

For the order analysis, the small parameters for the problem are first identified. For the case of the rectangular cross section beam, the width to length ratio, $\delta_b = \frac{b}{L}$ is the geometric small parameter, and for a slender rectangular beam $O(b) = O(h)$, where, h is the beam thickness. The geometric small parameters in the cross section along with the order of strain are included in the strain energy expression and subsequently, the cross-sectional strain energy terms are segregated in the order of their magnitudes. Taking strain to have a maximum order of $O(\epsilon)$ such that $\epsilon \ll 1$, the order analysis is carried out in this manner. Furthermore, the following constraints are applied on the warping variables in the VAM procedure:

$$\langle w_i \rangle = 0 \tag{24}$$

$$\langle x_2 w_3 - x_3 w_2 \rangle = 0 \tag{25}$$

Here, the notation $< >$ implies that the integration is carried out over the entire reference cross section. The first constraint physically implies that warping does not contribute to rigid body displacement of the cross section and the second implies the torsional rotation variable is the average rotation of the cross section about $\mathbf{B}_1$.

It is noted that the zeroth-order approximation to the strain energy should contain all terms up to the $O(E\,\epsilon^2)$, where $O(E)$ is the order of a typical 3-D stiffness coefficient. Also, for the first-order approximation, the terms taken in the strain energy approximation include all the terms from the zeroth-order approximation along with the higher-order terms up to $O\left(E\,\epsilon^2\delta_b^2\right)$. For both these cases, applying the energy principle, which states that the warping function satisfying the above constraints must minimise the strain energy

functional, the Euler-Lagrange equations are derived. These equations govern the problem definition and the associated boundary conditions. Solving the equations leads to the analytical warping solutions.

2.2.3. 1-D Beam Analysis

The 1-D analysis of beam focuses on getting the 1-D displacements and rotations using the results from the cross-sectional analysis in the ensuing VAM formulation process. Referring to Hodges [44], the Euler-Lagrange equations for a prismatic beam in static state is obtained as:

$$F' + f^d = 0 \tag{26}$$
$$M' + \tilde{e_1} F + m^d = 0 \tag{27}$$

where, F and M are the force and moment column matrices and each comprise of force and moment components along the three coordinates. These can be represented as $F = [F_1, F_2, F_3]$ and $M = [M_1, M_2, M_3]$. Also, f^d is the distributed force matrix ($f^d = [f_1^d, f_2^d, f_3^d]$) and m^d represents the distributed moment matrix ($m^d = [m_1^d, m_2^d, m_3^d]$). Here, $\tilde{e_1}$ is given as follows:

$$\tilde{e_1} = \begin{bmatrix} 0 & 0 & 0 \\ 0 & 0 & -1 \\ 0 & 1 & 0 \end{bmatrix} \tag{28}$$

Now, the 1-D strains and curvatures are related to the displacements (in this case u) and rotations (θ) using the following kinematic relations [45]:

$$\gamma = u' + \tilde{e_1}\theta \tag{29}$$
$$\kappa = \theta' \tag{30}$$

where, $\gamma = [\gamma_{11}, 2\gamma_{12}, 2\gamma_{13}]$ and $\kappa = [\kappa_1, \kappa_2, \kappa_3]$, the physical meaning of these components has been explained in the previous section. Further, the displacement and rotation matrices comprise the components, $u = [u_1, u_2, u_3]$ and $\theta = [\theta_1, \theta_2, \theta_3]$. The above relation is obtained for the current case from the intrinsic kinematic formulation in [45]. The relation between the generalised strain measures and kinematic quantities can be represented by:

$$\boldsymbol{\gamma} = \boldsymbol{C}^{bB}.\boldsymbol{R}' - \boldsymbol{r}' \tag{31a}$$
$$\boldsymbol{\kappa} = \boldsymbol{C}^{bB}.\boldsymbol{K} - \boldsymbol{k} \tag{31b}$$

In the above equations, the curvature vector of the deformed reference line is represented by $\boldsymbol{K}$ whereas $\boldsymbol{k}$ is the curvature vector of the undeformed reference line. Also, the following representation follows:

$$\tilde{\boldsymbol{K}} = (\boldsymbol{C}^{BA})'.\boldsymbol{C}^{AB} \tag{32a}$$
$$\tilde{\boldsymbol{k}} = \left(\boldsymbol{C}^{bA}\right)'.\boldsymbol{C}^{Ab} \tag{32b}$$

Here, A represents the reference frame, which is an absolute frame in which the orientation of the local undeformed beam cross section is only a function of x_1. From the above equations, the following relations can be obtained as [45]:

$$\gamma = C\left(e_1 + u' + \tilde{k}u\right) - e_1 \tag{33a}$$
$$\kappa = K - k \tag{33b}$$

Here, C is the direction cosine matrix, $\tilde{K} = -C'C^T + C\tilde{k}C^T$ and $k = [k_1, k_2, k_3]$. Also, here $e_1 = [1 \quad 0 \quad 0]^T$. Further simplification yield:

$$\gamma = u' + \tilde{k}u + \tilde{e_1}\theta \tag{34a}$$
$$\kappa = \theta' + \tilde{k}\theta \tag{34b}$$

In the present work, with no initial curvatures considered, these relations reduce to the form as seen in Eq. 29-30. Further details relating to the kinematics can be found in [44, 45] and have not been included here as it does not add to the present work. It is also known from [44] that the generalised force and moments are given by the following relations:

$$F = \frac{\partial U}{\partial \gamma_{11}} \tag{35}$$
$$M_i = \frac{\partial U}{\partial \kappa_i} \tag{36}$$

Applying cantilever boundary conditions, i.e., keeping one end fixed and other end free, the following force and moment components were obtained:

$$F = \begin{Bmatrix} \widehat{F_1} + f_1^d(L - x_1) \\ \widehat{F_2} + f_2^d(L - x_1) \\ \widehat{F_3} + f_3^d(L - x_1) \end{Bmatrix} \tag{37}$$

$$M = \begin{Bmatrix} \widehat{M_1} + m_1^d(L - x_1) \\ \widehat{M_2} - \frac{1}{2}(L - x_1)(f_3^d(L - x_1) + 2(\widehat{F_3} - m_2^d)) \\ \widehat{M_3} + \frac{1}{2}(L - x_1)(f_2^d(L - x_1) + 2(\widehat{F_2} + m_3^d)) \end{Bmatrix} \tag{38}$$

Here, $\widehat{F_1}$, $\widehat{F_2}$, $\widehat{F_3}$ and $\widehat{M_1}$, $\widehat{M_2}$, $\widehat{M_3}$ represent the tip forces and moments respectively along the three coordinate directions. L represents the total length of the beam whereas, x_1 represents the coordinate location along the beam length.

3. Methodology

Using VAM-based kinematic expressions, which relate the deformations at a position in the beam to the position coordinates, the kinematic expressions for 3-D strains and the derivatives of strains were obtained. The idea is to use the strain energy density formulation from strain gradient theory (Eq.2) instead of the conventional strain energy density expression (Eq.23). The derived new strain energy density expression is then segregated into the orders of small parameters. Carrying out the order analysis, the variational formulation is applied and Euler-Lagrange partial differential equations and boundary conditions are obtained, which are solved to determine the warping solutions of the cross section. The new strain energy density expression is divided into constituent strain energy density terms based on their origin as given in Eq.39. and can be written as follows:

$$U = \underbrace{\frac{1}{2}\int \sigma_{ij}\varepsilon_{ij}}_{U_{classical}} + \underbrace{\frac{1}{2}\int p_i\gamma_i}_{U_{higher1}} + \underbrace{\frac{1}{2}\int \tau^{(1)}_{ijk}\eta^{(1)}_{ijk}}_{U_{higher2}} + \underbrace{\frac{1}{2}\int m^s_{ij}X^s_{ij}}_{U_{higher3}} \tag{39}$$

Now, for consideration of the strain gradient energy for VAM treatment, the higher-order strain terms in Eq.39 are evaluated. From the higher-order strain definitions as given in [49], it can be shown that,

$$\gamma_i = \partial_i\Gamma_{mm} = \frac{\partial(\Gamma_{11}+\Gamma_{22}+\Gamma_{33})}{\partial x_i} \tag{40}$$

The deviatoric stretch gradient tensor is derived for the VAM based formulation using the following relation:

$$\eta^{(1)}_{ijk} = \eta^s_{ijk} - \frac{1}{5}\left(\delta_{ij}\eta^s_{ppk} + \delta_{ik}\eta^s_{ppj} + \delta_{jk}\eta^s_{ppi}\right) \tag{41}$$

where, $\eta^s_{ijk} = \frac{1}{3}(\eta_{ijk} + \eta_{jki} + \eta_{kij})$ is the symmetric part of the tensor η_{ijk}. And, $\eta_{ijk} = \varepsilon_{jk,i} + \varepsilon_{ki,j} - \varepsilon_{ij,k}$,which is equivalent to the following expression,

$$\eta_{ijk} = \Gamma_{jk,i} + \Gamma_{ki,j} - \Gamma_{ij,k} \tag{42}$$

From the above expressions, the following components of the deviatoric stretch gradient tensor are obtained:

$$\eta^{(1)}_{111} = \frac{2}{5}\left(\frac{\partial\Gamma_{11}}{\partial x_1}\right) - \frac{1}{5}\left(\frac{\partial\Gamma_{22}}{\partial x_1} + \frac{\partial\Gamma_{33}}{\partial x_1} + 2\frac{\partial\Gamma_{12}}{\partial x_2} + 2\frac{\partial\Gamma_{13}}{\partial x_3}\right) \tag{43a}$$

$$\eta^{(1)}_{222} = \frac{2}{5}\left(\frac{\partial\Gamma_{22}}{\partial x_2}\right) - \frac{1}{5}\left(\frac{\partial\Gamma_{11}}{\partial x_2} + \frac{\partial\Gamma_{33}}{\partial x_2} + 2\frac{\partial\Gamma_{12}}{\partial x_1} + 2\frac{\partial\Gamma_{23}}{\partial x_3}\right) \tag{43b}$$

$$\eta^{(1)}_{333} = \frac{2}{5}\left(\frac{\partial\Gamma_{33}}{\partial x_3}\right) - \frac{1}{5}\left(\frac{\partial\Gamma_{11}}{\partial x_3} + \frac{\partial\Gamma_{22}}{\partial x_3} + 2\frac{\partial\Gamma_{13}}{\partial x_1} + 2\frac{\partial\Gamma_{23}}{\partial x_2}\right) \tag{43c}$$

$$\eta^{(1)}_{123} = \eta^{(1)}_{132} = \eta^{(1)}_{321} = \eta^{(1)}_{312} = \eta^{(1)}_{231} = \eta^{(1)}_{213} = \frac{1}{3}\left(\frac{\partial\Gamma_{12}}{\partial x_3} + \frac{\partial\Gamma_{13}}{\partial x_2} + \frac{\partial\Gamma_{23}}{\partial x_1}\right) \tag{43d}$$

$$\eta^{(1)}_{112} = \eta^{(1)}_{211} = \eta^{(1)}_{121} = \frac{1}{3}\left(2\frac{\partial\Gamma_{12}}{\partial x_1} + \frac{\partial\Gamma_{11}}{\partial x_2}\right) - \frac{1}{15}\left(\frac{\partial\Gamma_{11}}{\partial x_2} + 3\frac{\partial\Gamma_{22}}{\partial x_2} + \frac{\partial\Gamma_{33}}{\partial x_2} + 2\frac{\partial\Gamma_{12}}{\partial x_1} + 2\frac{\partial\Gamma_{23}}{\partial x_3}\right) \tag{43e}$$

$$\eta^{(1)}_{113} = \eta^{(1)}_{311} = \eta^{(1)}_{131} = \frac{1}{3}\left(2\frac{\partial\Gamma_{13}}{\partial x_1} + \frac{\partial\Gamma_{11}}{\partial x_3}\right) - \frac{1}{15}\left(\frac{\partial\Gamma_{11}}{\partial x_3} + \frac{\partial\Gamma_{22}}{\partial x_3} + 3\frac{\partial\Gamma_{33}}{\partial x_3} + 2\frac{\partial\Gamma_{13}}{\partial x_1} + 2\frac{\partial\Gamma_{23}}{\partial x_2}\right) \tag{43f}$$

$$\eta^{(1)}_{122} = \eta^{(1)}_{212} = \eta^{(1)}_{221} = \frac{1}{3}\left(2\frac{\partial\Gamma_{12}}{\partial x_2} + \frac{\partial\Gamma_{22}}{\partial x_1}\right) - \frac{1}{15}\left(3\frac{\partial\Gamma_{11}}{\partial x_1} + \frac{\partial\Gamma_{22}}{\partial x_1} + \frac{\partial\Gamma_{33}}{\partial x_1} + 2\frac{\partial\Gamma_{12}}{\partial x_2} + 2\frac{\partial\Gamma_{13}}{\partial x_3}\right) \tag{43g}$$

$$\eta^{(1)}_{133} = \eta^{(1)}_{313} = \eta^{(1)}_{331} = \frac{1}{3}\left(2\frac{\partial\Gamma_{13}}{\partial x_3} + \frac{\partial\Gamma_{33}}{\partial x_1}\right) - \frac{1}{15}\left(3\frac{\partial\Gamma_{11}}{\partial x_1} + \frac{\partial\Gamma_{22}}{\partial x_1} + \frac{\partial\Gamma_{33}}{\partial x_1} + 2\frac{\partial\Gamma_{12}}{\partial x_2} + 2\frac{\partial\Gamma_{13}}{\partial x_3}\right) \tag{43h}$$

$$\eta^{(1)}_{223} = \eta^{(1)}_{232} = \eta^{(1)}_{322} = \frac{1}{3}\left(2\frac{\partial\Gamma_{23}}{\partial x_2} + \frac{\partial\Gamma_{22}}{\partial x_3}\right) - \frac{1}{15}\left(\frac{\partial\Gamma_{11}}{\partial x_3} + \frac{\partial\Gamma_{22}}{\partial x_3} + 3\frac{\partial\Gamma_{33}}{\partial x_3} + 2\frac{\partial\Gamma_{23}}{\partial x_2} + 2\frac{\partial\Gamma_{13}}{\partial x_1}\right) \tag{43i}$$

$$\eta^{(1)}_{233} = \eta^{(1)}_{323} = \eta^{(1)}_{332} = \frac{1}{3}\left(2\frac{\partial\Gamma_{23}}{\partial x_3} + \frac{\partial\Gamma_{33}}{\partial x_2}\right) - \frac{1}{15}\left(\frac{\partial\Gamma_{11}}{\partial x_2} + 3\frac{\partial\Gamma_{22}}{\partial x_2} + \frac{\partial\Gamma_{33}}{\partial x_2} + 2\frac{\partial\Gamma_{12}}{\partial x_1} + 2\frac{\partial\Gamma_{23}}{\partial x_3}\right) \tag{43j}$$

Also, the symmetric rotation gradient tensor is obtained as: $X^s_{ij} = \frac{1}{4}(e_{ipq}\eta_{jpq} + e_{jpq}\eta_{ipq})$, the components of which are as follows:

$$X^s_{11} = \frac{\partial\Gamma_{13}}{\partial x_2} - \frac{\partial\Gamma_{12}}{\partial x_3} \tag{44a}$$

$$X_{22}^{s} = \frac{\partial \Gamma_{12}}{\partial x_3} - \frac{\partial \Gamma_{23}}{\partial x_1} \tag{44b}$$

$$X_{33}^{s} = \frac{\partial \Gamma_{23}}{\partial x_1} - \frac{\partial \Gamma_{13}}{\partial x_2} \tag{44c}$$

$$X_{12}^{s} = \frac{1}{2}\left(\frac{\partial \Gamma_{23}}{\partial x_2} - \frac{\partial \Gamma_{22}}{\partial x_3} + \frac{\partial \Gamma_{11}}{\partial x_3} - \frac{\partial \Gamma_{13}}{\partial x_1}\right) \tag{44d}$$

$$X_{13}^{s} = \frac{1}{2}\left(\frac{\partial \Gamma_{12}}{\partial x_1} - \frac{\partial \Gamma_{11}}{\partial x_2} + \frac{\partial \Gamma_{33}}{\partial x_2} - \frac{\partial \Gamma_{23}}{\partial x_3}\right) \tag{44e}$$

$$X_{23}^{s} = \frac{1}{2}\left(\frac{\partial \Gamma_{22}}{\partial x_1} - \frac{\partial \Gamma_{33}}{\partial x_1} + \frac{\partial \Gamma_{13}}{\partial x_3} - \frac{\partial \Gamma_{12}}{\partial x_2}\right) \tag{44f}$$

Once the higher-order strain terms have been obtained, the components are substituted into the strain energy expression given by Eq.39. and the variational approach of minimizing the strain energy functional to obtain the governing Euler-Lagrange equations for warping estimation is instigated.

The first question which arises with the above implementation, is the order of the material length- scale parameter. This is a fundamental question which is addressed here by taking three different cases for the order of length-scale parameters by considering that $l_o, l_1, l_2 = l$. Here, all of them are taken to be equal as has been the common practice in the literature [25, 26, 29]. The consequence of these choices is summarised below.

(a) Order of material length-scale parameter less than the cross-sectional parameter ($\boldsymbol{O(l) \ll O(b)}$)

Since length-scale parameters depict the material microstructure behaviour, it is reasonable to assume that their order can be less than the order of the beam width or height, which are the cross-sectional (geometric) parameters. With this approximation, a new small parameter, as the ratio of the material length-scale parameter to the cross-sectional dimension of the beam (here the width), $\delta_m = \frac{l}{b} \ll 1$, is defined and is associated with the material length-scale parameters. With this new small parameter, along with the classical small parameter of beam width to length ratio i.e., δ_b, the VAM procedure and separation of the strain energy functional in terms of the orders of small parameters are carried out. For the zeroth-order approximation the following strain energy terms can be obtained,

$$U_{Classical} = \underbrace{\frac{E(\nu-1)(\gamma_{11}^2+x_3^2\kappa_2^2+x_2^2\kappa_3^2+{w_{2,2}}^2+{w_{3,3}}^2)}{2(2\nu^2+\nu-1)} + \frac{E({w_{1,2}}^2+{w_{1,3}}^2+{w_{2,3}}^2+{w_{3,2}}^2)}{4(1+\nu)} + \cdots}_{\boldsymbol{O(E\epsilon^2)}} + O(E\epsilon^2\delta_b) + O\left(E\epsilon^2\delta_b^2\right) \tag{45a}$$

$$U_{higher1} = \overbrace{\frac{El_o^2(\kappa_2^2+\kappa_3^2)}{2(1+\nu)} + \frac{El_o^2\kappa_2 w_{3,33}}{(1+\nu)} + \frac{El_o^2{w_{3,33}}^2}{2(1+\nu)} + + \frac{El_o^2\kappa_2 w_{2,23}}{(1+\nu)} + \frac{El_o^2{w_{2,23}}^2}{2(1+\nu)} + \cdots \ldots}^{\boldsymbol{O(E\epsilon^2\delta_m^2)}} + O(E\epsilon^2\delta_m^2\delta_b) + O\left(E\epsilon^2\delta_m^2\delta_b^2\right) + O\left(E\epsilon^2\delta_m^2\delta_b^3\right) + O\left(E\epsilon^2\delta_m^2\delta_b^4\right) \tag{45b}$$

$$U_{higher2} = \underbrace{\frac{9El_1^2(\kappa_2^2+\kappa_3^2)}{25(1+\nu)} + \frac{9El_1^2({w_{1,33}}^2+{w_{2,33}}^2)}{25(1+\nu)} + \frac{7El_1^2\kappa_3 w_{2,33}}{25(1+\nu)} - \frac{11El_1^2\kappa_2 w_{3,33}}{25(1+\nu)} + \frac{11El_1^2{w_{3,33}}^2}{25(1+\nu)} + \cdots +}_{\boldsymbol{O(E\epsilon^2\delta_m^2)}}$$

$$O(E\epsilon^2\delta_m^2\delta_b) + O\left(E\epsilon^2\delta_m^2\delta_b^2\right) + O\left(E\epsilon^2\delta_m^2\delta_b^3\right) + O\left(E\epsilon^2\delta_m^2\delta_b^4\right) \tag{45c}$$

$$U_{higher3} = \overbrace{\frac{El_2^2\{3\kappa_1^2+2(\kappa_2^2+\kappa_3^2)\}}{4(1+\nu)} + \frac{El_2^2(w_{1,33}{}^2+w_{2,33}{}^2)}{8(1+\nu)} + \frac{El_2^2(2w_{1,23}{}^2+w_{2,23}{}^2+w_{3,23}{}^2)}{8(1+\nu)} - \frac{El_2^2 w_{2,33}w_{3,23}}{4(1+\nu)} + \ldots}^{\boldsymbol{O(E\epsilon^2\delta_m^2)}} + O(E\epsilon^2\delta_m^2\delta_b) + O\left(E\epsilon^2\delta_m^2\delta_b^2\right) + O\left(E\epsilon^2\delta_m^2\delta_b^3\right) + O\left(E\epsilon^2\delta_m^2\delta_b^4\right) \tag{45d}$$

It is evident from the above equations that due to the additional small parameter, except for the classical strain energy ($O(E\epsilon^2)$), the strain gradient strain energy terms are of the order $O(E\epsilon^2\delta_m^2)$ which represent higher-order terms than the one which appear in the zeroth-order approximation. Hence the procedure will not be able to capture the size effects at the zeroth-order or even at the first-order approximation. Naturally, the zeroth-order and first-order approximations will result in classical beam results only. It is therefore, obvious that such a choice of material length-scale parameters will not be effective in capturing the small-scale effects because the zeroth-order approximation gives essentially the classical results.

(b) Order of the material length-scale parameter equal to the order of length of the beam ($\boldsymbol{O(l) = O(L)}$)

Now, the case when the order of material length-scale parameters has the same order as that of the beam length is explored. There are relatively few but some relevant literature which reports results for the case where $\boldsymbol{l/L}$ is essentially taken as one [50, 51]. However, it is seen that for this case, the classical strain energy remains more or less unaffected. However, the strain energy associated with the strain gradients show the terms to be larger than the ones in the classical strain energy. This can be vindicated by the following strain energy expressions along with the orders for the different terms. Here, δ_b is the small parameter representing the ratio of beam width to its length.

$$U_{Classical} = \underbrace{\frac{E(\nu-1)(\gamma_{11}^2+x_3^2\kappa_2^2+x_2^2\kappa_3^2+w_{2,2}{}^2+w_{3,3}{}^2)}{2(2\nu^2+\nu-1)} + \frac{E(w_{1,2}{}^2+w_{1,3}{}^2+w_{2,3}{}^2+w_{3,2}{}^2)}{4(1+\nu)} + \cdots}_{\boldsymbol{O(E\epsilon^2)}} + O(E\epsilon^2\delta_b) + O\left(E\epsilon^2\delta_b^2\right) \tag{46a}$$

$$U_{higher1} = \underbrace{\frac{El_o^2(\kappa_2^2+\kappa_3^2)}{2(1+\nu)} + \frac{El_o^2\kappa_2 w_{3,33}}{(1+\nu)} + \frac{El_o^2 w_{3,33}{}^2}{2(1+\nu)} + + \frac{El_o^2\kappa_2 w_{2,23}}{(1+\nu)} + \frac{El_o^2 w_{2,23}{}^2}{2(1+\nu)} + \cdots\ldots +}_{\boldsymbol{O\left(E\frac{\epsilon^2}{\delta_b^2}\right)}} \underbrace{\frac{El_o^2\kappa_2 w_{1,13}}{1+\nu} + \frac{El_o^2 w_{3,33}w_{1,13}}{1+\nu} + \frac{El_o^2 w_{2,23}w_{1,13}}{1+\nu} + \cdots +}_{\boldsymbol{O\left(E\frac{\epsilon^2}{\delta_b}\right)}}$$

$$\underbrace{\frac{El_o^2({w_{1,13}}^2+{w_{3,13}}^2+{w_{1,12}}^2+{w_{2,12}}^2)}{2(1+\nu)}+\frac{El_o^2 w_{2,12}w_{3,13}}{1+\nu}}_{\boldsymbol{O(E\epsilon^2)}}+O(E\epsilon^2\delta_b)+$$
$$O\left(E\epsilon^2\delta_b^2\right) \tag{46b}$$

$$U_{higher2}=$$
$$\underbrace{\frac{9El_1^2(\kappa_2^2+\kappa_3^2)}{25(1+\nu)}+\frac{9El_1^2({w_{1,33}}^2+{w_{2,33}}^2)}{25(1+\nu)}+\frac{7El_1^2\kappa_3 w_{2,33}}{25(1+\nu)}-\frac{11El_1^2\kappa_2 w_{3,33}}{25(1+\nu)}+\frac{11El_1^2{w_{3,33}}^2}{25(1+\nu)}+\cdots}_{\boldsymbol{O\left(E\frac{\epsilon^2}{\delta_b^2}\right)}}+$$
$$\underbrace{\frac{36El_1^2\kappa_2 w_{1,13}}{25(1+\nu)}-\frac{22El_1^2 w_{3,33}w_{1,13}}{25(1+\nu)}+\frac{28El_1^2 w_{3,23}w_{1,13}}{25(1+\nu)}+\cdots.}_{\boldsymbol{O\left(E\frac{\epsilon^2}{\delta_b}\right)}}+$$
$$\underbrace{\frac{36El_1^2({w_{1,13}}^2+{w_{1,12}}^2)}{25}-\frac{28El_1^2 w_{3,13}w_{2,12}}{25(1+\nu)}+\cdots..}_{\boldsymbol{O(E\epsilon^2)}}+O(E\epsilon^2\delta_b)+$$
$$O\left(E\epsilon^2\delta_b^2\right) \tag{46c}$$

$$U_{higher3}=\underbrace{\frac{El_2^2\{3\kappa_1^2+2(\kappa_2^2+\kappa_3^2)\}}{4(1+\nu)}+\frac{El_2^2({w_{1,33}}^2+{w_{2,33}}^2)}{8(1+\nu)}-\frac{El_2^2 w_{1,22}w_{1,33}}{4(1+\nu)}+\cdots....}_{\boldsymbol{O\left(E\frac{\epsilon^2}{\delta_b^2}\right)}}+$$
$$\underbrace{\frac{El_2^2\kappa_2 w_{1,13}}{2(1+\nu)}-\frac{El_2^2\kappa_3 w_{1,12}}{2(1+\nu)}-\frac{El_2^2 w_{1,23}w_{2,13}}{4(1+\nu)}+\cdots..}_{\boldsymbol{O\left(E\frac{\epsilon^2}{\delta_b}\right)}}+$$
$$\underbrace{\frac{El_2^2({w_{1,13}}^2+2{w_{2,13}}^2+{w_{3,13}}^2)}{8(1+\nu)}-\frac{El_2^2\kappa_2 w_{3,11}}{2(1+\nu)}+\cdots..}_{\boldsymbol{O(E\epsilon^2)}}+O(E\epsilon^2\delta_b)+$$
$$O\left(E\epsilon^2\delta_b^2\right) \tag{46d}$$

Thus, terms with orders $O\left(E\frac{\epsilon^2}{\delta_b^2}\right), O\left(E\frac{\epsilon^2}{\delta_b}\right)$ along with the $O(E\epsilon^2)$ and other larger terms which have order lower than the classical strain energy form are retained. It is known that such a phenomenon occurs when there are certain terms in the strain that are larger in magnitude than the corresponding strain component itself. The problem is solved by balancing these terms with an equally large term such that their combination results in a smaller order. These terms are called 'Phantom' terms. In the VAM procedure, these terms are minimised to zero, and the process is referred to as the killing of the large terms. Since this is happening for the strain gradient terms, the phantom step needs to be applied for the gradient terms in order to solve this variational problem statement. It is necessary to use Phantom step [44] to eliminate/kill these lower order terms and then proceed with zeroth-order approximation as usual for the VAM approach to be effective. This forms a different set of problem definitions that can be looked at as an intriguing, but worthwhile exercise in future works. It is expected to provide further insights into the material length-scale parameters. However, this is out of the scope of this paper.

(c) Order of the material length-scale parameter equal to the cross-sectional parameter ($O(l) = O(b)$)

It is seen that for this order of the length-scale parameters, the classical strain energy terms as well as the strain gradient terms appear into the zeroth-order terms constituting the overall strain energy of the beam, presenting it as an appropriate choice. The zeroth-order is also evident in a substantial majority of the literature wherein the width and length-scale parameters are in micrometres or nanometres [25, 28, 49]. With such observations, it is ascertained that the development of the strain gradient beam model with this choice for the length-scale parameters is a step in the right direction. Taking, δ_b as the small parameter representing the ratio of beam width to length, the following strain energy expression is obtained from this case:

$$U_{Classical} = \underbrace{\frac{E(v-1)(\gamma_{11}^2+x_3^2\kappa_2^2+x_2^2\kappa_3^2+{w_{2,2}}^2+{w_{3,3}}^2)}{2(2v^2+v-1)} + \frac{E({w_{1,2}}^2+{w_{1,3}}^2+{w_{2,3}}^2+{w_{3,2}}^2)}{4(1+v)} + \cdots}_{\boldsymbol{O(E\epsilon^2)}} + O(E\epsilon^2\delta_b) + O\left(E\epsilon^2\delta_b^2\right) \tag{47a}$$

$$U_{higher1} = \underbrace{\frac{El_o^2(\kappa_2^2+\kappa_3^2)}{2(1+v)} + \frac{El_o^2 w_{3,33}w_{2,23}}{1+v} + \frac{El_o^2 w_{3,23}w_{2,22}}{1+v} - \frac{El_o^2\kappa_3 w_{2,22}}{1+v} + \cdots .}_{\boldsymbol{O(E\epsilon^2)}} + \underbrace{\frac{El_o^2\kappa_2 w_{1,12}}{1+v} + \frac{El_o^2 w_{3,33}w_{1,13}}{1+v} + \cdots}_{\boldsymbol{O(E\epsilon^2\delta_b)}} + \underbrace{\frac{El_o^2({w_{1,13}}^2+{w_{3,13}}^2+{w_{1,12}}^2+{w_{2,12}}^2)}{2(1+v)} + \frac{El_o^2 w_{3,13}w_{2,12}}{1+v}}_{\boldsymbol{O(E\epsilon^2\delta_b^2)}} + \underbrace{\frac{El_o^2 w_{1,11}(w_{3,13}+w_{2,12})}{1+v}}_{\boldsymbol{O(E\epsilon^2\delta_b^3)}} + \underbrace{\frac{El_o^2 {w_{1,11}}^2}{2(1+v)}}_{\boldsymbol{O(E\epsilon^2\delta_b^4)}} \tag{47b}$$

$$U_{higher2} = \underbrace{\frac{9El_1^2(\kappa_2^2+\kappa_3^2)}{25(1+v)} + \frac{9El_1^2({w_{1,33}}^2+{w_{2,33}}^2)}{25(1+v)} + \frac{7El_1^2\kappa_3 w_{2,33}}{25(1+v)} + \cdots .}_{\boldsymbol{O(E\epsilon^2)}} + \underbrace{\frac{36El_1^2\kappa_2 w_{1,13}}{25(1+v)} - \frac{22El_1^2 w_{3,33}w_{1,13}}{25(1+v)} - \frac{14El_1^2 w_{3,22}w_{1,13}}{25(1+v)} + \cdots}_{\boldsymbol{O(E\epsilon^2\delta_b)}} + \underbrace{\frac{36El_1^2({w_{1,12}}^2+{w_{1,13}}^2+{w_{2,12}}^2+{w_{3,13}}^2)}{25(1+v)} + \frac{4El_1^2 w_{2,13}w_{3,12}}{1+v} + \cdots ..}_{\boldsymbol{O(E\epsilon^2\delta_b^2)}} - \underbrace{\frac{22El_1^2 w_{1,11}(w_{2,12}+w_{3,13})}{25(1+v)}}_{\boldsymbol{O(E\epsilon^2\delta_b^3)}} + \underbrace{\frac{El_1^2\{11({w_{1,11}}^2+9({w_{2,11}}^2+{w_{3,11}}^2)\}}{25(1+v)}}_{\boldsymbol{O(E\epsilon^2\delta_b^4)}} \tag{47c}$$

$$U_{higher3} = \underbrace{\frac{El_2^2\{3\kappa_1^2+2(\kappa_2^2+\kappa_3^2)\}}{4(1+v)} + \frac{El_2^2({w_{1,33}}^2+{w_{2,33}}^2)}{8(1+v)} - \frac{El_2^2 w_{1,22}w_{1,33}}{4(1+v)} + \cdots .}_{\boldsymbol{O(E\epsilon^2)}} + \underbrace{\frac{El_2^2\kappa_2 w_{1,13}}{2(1+v)} - \frac{El_2^2 w_{2,23}w_{1,13}}{4(1+v)} + \frac{El_2^2 w_{3,22}w_{1,13}}{4(1+v)} + \cdots .}_{\boldsymbol{O(E\epsilon^2\delta_b)}} +$$

$$\underbrace{\frac{El_2^2(w_{1,13}{}^2+2w_{2,13}{}^2+w_{3,13}{}^2+w_{1,12}{}^2+w_{2,12}{}^2+2w_{3,12}{}^2)}{8(1+v)}+\cdots.}_{\boldsymbol{O(E\epsilon^2\delta_b^2)}}-$$
$$\underbrace{\frac{El_2^2(w_{1,12}w_{2,11}+w_{1,13}w_{3,11})}{4(1+v)}}_{\boldsymbol{O(E\epsilon^2\delta_b^3)}}+\underbrace{\frac{El_2^2(w_{2,11}{}^2+w_{3,11}{}^2)}{8(1+v)}}_{\boldsymbol{O(E\epsilon^2\delta_b^4)}} \tag{47d}$$

Here, the case is that O (l)=O (b) and the following fourth-order partial differential equation for the zeroth-order approximation are obtained.

$$(72l_1^2+25l_2^2)(w_{1,2222}+w_{1,3333})+344l_1^2w_{1,2233}-50\big(w_{1,22}+w_{1,33}\big)=0 \tag{48}$$

$$4(2v-1)(22l_1^2+25l_o^2)w_{2,2222}+25(2v-1)(4l_o^2+8l_1^2+l_2^2)w_{2,2233}+(2v-1)(72l_1^2+25l_2^2)w_{2,3333}+(2v-1)(56l_1^2-25(l_2^2-4l_o^2))(w_{3,2333}+w_{3,2223})-50(2v-1)w_{2,33}-100(v-1)w_{2,22}+50w_{3,23}-100v\kappa_3=0 \tag{49}$$

$$4(2v-1)(22l_1^2+25l_o^2)w_{3,3333}+25(2v-1)(4l_o^2+8l_1^2+l_2^2)w_{3,2233}+(2v-1)(72l_1^2+25l_2^2)w_{3,2222}+(2v-1)(56l_1^2-25(l_2^2-4l_o^2))(w_{2,2333}+w_{2,2223})+50(2v-1)w_{3,22}-100(v-1)w_{3,33}+50w_{2,23}+100v\kappa_2=0 \tag{50}$$

and the associated boundary conditions are:

$$n_2\big(w_{1,2}-x_3\kappa_1\big)+n_3(w_{1,3}+x_2\kappa_1)=0 \tag{51}$$

$$n_3\big(w_{2,3}+w_{3,2}\big)+\frac{2n_2}{(1-2v)}(v(\gamma_{11}+x_3\kappa_2-x_2\kappa_3)+(1-v)w_{2,2}+vw_{3,3})=0 \tag{52}$$

$$n_2\big(w_{2,3}+w_{3,2}\big)+\frac{2n_3}{(1-2v)}(v(\gamma_{11}+x_3\kappa_2-x_2\kappa_3)+vw_{2,2}+(1-v)w_{3,3})=0 \tag{53}$$

These are the classical boundary conditions, but due to higher-order strain terms present in the new strain energy definition, additional non classical higher-order boundary conditions are also obtained and are as follows:

$$n_2\frac{13\,l_1^2}{2}\big(w_{1,23}\big)+n_3\frac{l_1^2}{200}(97\,w_{1,33}-106\,w_{1,22})=0 \tag{54}$$

$$n_2\frac{l_2^2}{200}(-6\,w_{1,33}+97\,w_{1,22})=0 \tag{55}$$

$$n_3\{w_{3,33}(25l_o^2+22l_1^2)+w_{2,23}(25l_o^2-22l_1^2)+\kappa_2(25l_o^2-11l_1^2)-11l_1^2\,w_{3,22}\}=0 \tag{56}$$

$$n_3\big\{(50l_o^2+25l_2^2+144l_1^2)w_{3,23}+2w_{2,22}(25l_o^2-22l_1^2)+w_{2,33}(72l_1^2-25l_o^2)+2\kappa_3(14l_1^2-25l_o^2)\big\}+n_2\{2(25l_2^2-18l_1^2)w_{3,22}+(25l_2^2+72l_1^2)w_{2,23}-22l_1^2w_{3,33}-(25l_2^2+7l_1^2)\kappa_2\}=0 \tag{57}$$

$$n_3\{w_{2,33}(25l_2^2+72l_1^2)+w_{3,23}(144l_1^2-25l_2^2)+2\kappa_2(14l_1^2-25l_2^2)-72l_1^2\,w_{2,33}\}=0 \tag{58}$$

$$n_3\big\{(100l_o^2+25l_2^2+288l_1^2)w_{2,23}+w_{3,33}(100l_o^2-8l_1^2)+w_{3,22}(144l_1^2-25l_2^2)+\kappa_2(100l_o^2-50l_2^2-14l_1^2)\big\}+n_2(-44l_1^2w_{2,33}-88l_1^2w_{3,23}+88l_1^2w_{2,22}+44l_1^2\kappa_3)=0 \tag{59}$$

Here, n_2 and n_3 represent the direction cosines of outward normal with respect to x_2 and x_3 respectively. By setting the material length-scale parameters to zero, i.e. $l_o = l_1 = l_2 = 0$, the above-defined boundary value problem reduces to that of the classical case, wherein strain gradient effects are not accounted for.

Based on the work by Barretta et al. [52], it appears that the inclusion of higher-order boundary conditions may not be essential to obtain a valid solution, as there remains uncertainty regarding their physical implications. However, other studies [53-55] have offered physical interpretations, suggesting that these boundary conditions could correspond to secondary forces and moments. Nevertheless, it has been observed that adopting higher-order boundary conditions can result in an over-constrained beam model. The research by Barretta et al. [52] demonstrates that no higher-order boundary conditions, such as non-classical boundary conditions, are necessary to address the relevant gradient problems adequately. While these boundary conditions arise from the variational formulation and possess mathematical significance, their physical relevance to the problem at hand remains undefined. Thus, their inclusions may be redundant and do not contribute much to the understanding the physics involved. In a relevant investigation, Polizzotto [56] also supported the idea of the relaxation of higher-order (non-classical) boundary conditions for the case of beams and plates. In another work by Polizzotto [57], it was ascertained that these boundary conditions were nonstandard in character, meaning that their role was to suitably complete the differential description of the material constitutive law rather than conveying boundary data in the relevant boundary value problem. Amiot [32] also mentioned the formidable challenges to satisfy all requirements for higher-grade elastic beam models and finally suggested that the relaxation of constraints is the way forward. Therefore, classical boundary conditions have been employed in this study to address the boundary value problem (see, Eq. 51, 52, and 53).

Additionally, it must be mentioned that various sets of boundary conditions were considered, and solutions were explored to solve the boundary value problem at hand, satisfactorily. However, only the selected set utilised in this study accurately captures the constitutive nature of the beam problem. Other sets fail to converge to classical results when length-scale parameters are set to zero, producing inaccurate outcomes. These discrepancies in results with boundary condition selection have been highlighted in the literature. Shokrieh et al. [58] also acknowledged the discrepancies in boundary conditions within the context of strain gradient elasticity. They highlighted that different sets of boundary conditions can result in distinct static responses, emphasizing the importance of selecting appropriate boundary conditions that align with the physics of the specific problem at hand. Moreover, they noted that for sufficiently large dimensions, the solution may not converge to classical results, which is consistent with the findings of the current research. It has been observed that by varying the applied boundary conditions leads to differing results in the beam formulation. In their work dell'Isola and Misra [34] mentioned about k-forces, which can be described as quantities dual in work of the normal gradients of virtual displacements at the body faces, edges and wedge boundaries. This was derived for Nth gradient continua using the principle of virtual work. Their work advocated that multipolar boundary conditions emerge naturally from the principle of virtual work and can be further deduced as natural and essential using an integration by parts argument.

With the above pretext, the studies conducted by Zhu and Li [55] and Tang et al. [59] indicated that the influence of higher-order strain gradients was more significantly

affected by the material length-scale parameters rather than the specific use of higher or non-classical boundary conditions. This insightful observation adds another layer of understanding to the relationship between strain gradients, boundary conditions, and material properties. Thus, while the role of higher-order boundary conditions in beam analysis remains uncertain, this research supports the notion that selecting appropriate boundary conditions based on the problem's physics is crucial. It is to be noted that the current study needs to be continued for future improvements, especially to explore the non-classical boundary conditions in more detail and develop solution methods for improved accuracy of the results.

4. Results and Discussion

4.1. Warping field and strain gradient stiffness: Zeroth-Order Solution

A beam with rectangular cross section having width 'b' and thickness 'h', such that the dimensions b and h are comparable and of the same order, is considered. The order of the length-scale parameters l_o, l_1 and l_2 is taken to be equal (l_o= l_1= l_2=l) and as the same order as that of the cross-sectional dimensions. This is taken in line with the literature as substantiated in the previous section. Invoking the VAM procedure, the Euler-Lagrange PDEs obtained in the previous section are now solved. A power series approximation for the warping solutions has been made to solve the boundary value problem and get the following cross-sectional warping solutions at the zeroth-order approximation:

$$\begin{aligned} w_1^0 &= x_2 x_3 \kappa_1 \\ w_2^0 &= \frac{1}{24} v[-24x_2(\gamma_{11} + x_3\kappa_2) + 12\, x_2^2\kappa_3 + (h^2 - b^2 - 12x_3^2)\kappa_3] \\ w_3^0 &= \frac{1}{24} v[(h^2 - b^2 - 12x_2^2)\kappa_2 - 12\, x_3^2\kappa_2 - 24x_3(\gamma_{11} - x_2\kappa_3)] \end{aligned} \tag{60}$$

where, w_1^0, w_2^0 and w_3^0 are the zeroth-order warping along the x_1, x_2 and x_3 directions respectively. It is important to note that these solutions represent the optimal outcomes achievable at the zeroth-order level within the variational gradient formulation while still adhering to the non-negotiables of the physical model, namely global constraints, and classical boundary conditions. Further refinement is, of course, possible to incorporate more precise solutions, potentially including non-classical boundary conditions in future studies. However, it is worth noting that these current solutions stand as the best possible fit. Substituting the warping solutions in the strain energy expression, the zeroth-order 1-D constitutive law with the strain gradient beam stiffness matrix can be given as follows:

$$U_{1D0} = \frac{1}{2}\begin{Bmatrix}\gamma_{11}\\ \kappa_1\\ \kappa_2\\ \kappa_3\end{Bmatrix}^T \begin{bmatrix} E\,b\,h & 0 & 0 & 0 \\ 0 & \frac{E\,b\,h\,(b^2+24\,l_1^2+12\,l_2^2)}{6(1+v)} & 0 & 0 \\ 0 & 0 & S_{s330}(l_o,l_1,l_2) & 0 \\ 0 & 0 & 0 & S_{s440}(l_o,l_1,l_2) \end{bmatrix} \begin{Bmatrix}\gamma_{11}\\ \kappa_1\\ \kappa_2\\ \kappa_3\end{Bmatrix} \tag{61}$$

where,

$$S_{s330}(l_o,l_1,l_2) = \frac{E\,b\,h^3}{12} + \frac{E\,b\,h\,l_o^2\,(1-2v)^2}{(1+v)} + \frac{18\,E\,b\,h\,l_1^2\,(1+v)}{25} + E\,b\,h\,l_2^2\,(1+v)$$

$$S_{s440}(l_o,l_1,l_2) = \frac{E\,b^3h}{12} + \frac{E\,b\,h\,l_o^2\,(1-2v)^2}{(1+v)} + \frac{18\,E\,b\,h\,l_1^2\,(1+v)}{25} + E\,b\,h\,l_2^2\,(1+v)$$

Here, S_{s330} and S_{s440} are the bending stiffnesses. It is worth noting that incorporating strain gradient effects introduces additional stiffness terms in the beam stiffness matrix, compared to those typically seen when using the classical strain energy expression instead of the modified strain gradient theory. These additional terms are evident in the torsional and bending stiffnesses. Moreover, if the material length-scale parameters are set to zero i.e. $l_o = l_1 = l_2 = 0$, or in a physical sense the contribution of the strain gradient effects is removed, the 1-D constitutive law converges to the classical Euler Bernoulli beam results. Also, the length-scale parameters come into effect at the zeroth-order, underscoring the significance of incorporating higher-order effects when modelling micro and nano beams. Furthermore, when all the length-scale parameters are set to zero, the stiffness matrix converges to the classical stiffness matrix for a Euler-Bernoulli beam, which is also obtained in the VAM derivation for rectangular cross sections when the classical strain energy is used instead of the strain gradient strain energy. It should be noted that in this VAM derivation using classical strain energy, a power series approximation for warping has been employed to solve the classical boundary value problem. From Eq. 61, it is evident that the material length-scale parameters influence the torsional and bending stiffness terms, highlighting the importance of small-scale effects for these loading conditions. Physically, the inclusion of these parameters alters the response of micro and nano scale beams to these loading conditions, resulting in outcomes that differ from those predicted by classical theories. This demonstrates the necessity of considering small-size effects in the analysis of such structures.

4.2. Warping field and strain gradient stiffness: First-Order Solution

In order to obtain the first-order approximation of the strain-gradient beam model, the zeroth-order warping solutions are perturbed to include the next order higher terms at the energy level. It is worth mentioning that such perturbation works at the energy level and the kinematics of the warping field of the cross section is obtained as a natural solution rather than enforcing kinematic assumptions beforehand deriving a dimensionally reduced beam theory. The first-order perturbations can be given as:

$$\begin{aligned} w_1^f &= \underset{O(\epsilon)}{w_1^0} + \underset{O(\epsilon\delta_b)}{V_1} \\ w_2^f &= \underset{O(\epsilon)}{w_2^0} + \underset{O(\epsilon\delta_b)}{V_2} \\ w_3^f &= \underset{O(\epsilon)}{w_3^0} + \underset{O(\epsilon\delta_b)}{V_3} \end{aligned} \tag{62}$$

Here, w_1^f, w_2^f and w_3^f give the first-order warpings and V_1, V_2, V_3 are the higher-order perturbations of order $O(\epsilon\delta_b)$. Substituting these perturbed warping solutions into the strain energy functional, and repeating the same variational approach as in the zeroth-order approximation, the governing differential equations, and boundary conditions for the first-order formulation are obtained. The following equations represent the first-order energies obtained:

$$U^f_{classical} = \underbrace{\frac{1}{2}E\{\gamma_{11}^2 + \frac{2x_2^2\kappa_1^2}{1+v} + 2\gamma_{11}(x_3\kappa_2 - x_2\kappa_3) + (x_3\kappa_2 - x_2\kappa_3)^2\}}_{\boldsymbol{O(E\epsilon^2)}} + \underbrace{\frac{Ex_2\kappa_1 V_{1,3}}{1+v}}_{O(\mu\epsilon^2\delta_b)} + \underbrace{\frac{E({V_{1,3}}^2+{V_{2,3}}^2)}{4(1+v)} + \frac{E(v-1){V_{3,3}}^2}{2(2v^2+v-1)} - \frac{Ev\,V_{2,2}V_{3,3}}{2v^2+v-1} + \cdots}_{\boldsymbol{O(E\epsilon^2\delta_b^2)}}.+$$

$$\underbrace{\frac{EvV_{1,1}V_{3,3}}{2v^2+v-1}-\frac{EvV_{2,2}V_{1,1}}{2v^2+v-1}+\frac{E(V_{1,2}V_{2,1}+V_{1,3}V_{3,1})}{2(1+v)}}_{\boldsymbol{O(E\epsilon^2\delta_b^3)}}+$$
$$\underbrace{\frac{E\{2(v-1)V_{1,1}^2+(2v-1)(V_{2,1}^2+V_{3,1}^2)\}}{4(2v^2+v-1)}}_{\boldsymbol{O(E\epsilon^2\delta_b^4)}} \tag{63a}$$

$$U^f_{higher1}=\underbrace{\frac{E(1-2v)^2l_o^2(\kappa_2^2+\kappa_3^2)}{2(1+v)}}_{\boldsymbol{O(E\epsilon^2)}}+\underbrace{\frac{El_o^2(1-2v)\{\kappa_2(V_{3,33}+V_{2,23})-\kappa_3(V_{3,23}+V_{2,22})\}}{(1+v)}}_{\boldsymbol{O(E\epsilon^2\delta_b)}}+$$
$$\underbrace{\frac{El_o^2{V_{3,33}}^2}{2(1+v)}+\frac{El_o^2({V_{2,23}}^2+{V_{3,23}}^2)}{2(1+v)}+\frac{El_o^2V_{3,33}V_{2,23}}{1+v}+\cdots}_{\boldsymbol{O(E\epsilon^2\delta_b^2)}}+$$
$$\underbrace{\frac{El_o^2(V_{3,33}V_{1,13}+V_{2,23}V_{1,13}+V_{3,23}V_{1,12}+V_{2,22}V_{1,12})}{1+v}}_{\boldsymbol{O(E\epsilon^2\delta_b^3)}}+$$
$$\underbrace{\frac{El_o^2V_{3,13}V_{2,12}}{(1+v)}+\frac{El_o^2({V_{1,12}}^2+{V_{1,13}}^2+{V_{3,13}}^2+{V_{2,12}}^2)}{2(1+v)}}_{\boldsymbol{O(E\epsilon^2\delta_b^4)}}+\underbrace{\frac{El_o^2V_{1,11}(V_{3,13}+V_{2,12})}{1+v}}_{\boldsymbol{O(E\epsilon^2\delta_b^5)}}+$$
$$\underbrace{\frac{El_o^2{V_{1,11}}^2}{2(1+v)}}_{\boldsymbol{O(E\epsilon^2\delta_b^6)}} \tag{63b}$$

$$U^f_{higher2}=\underbrace{\frac{El_1^2\{50\kappa_1^2+9(1+v)^2(\kappa_2^2+\kappa_3^2)\}}{25(1+v)}}_{\boldsymbol{O(E\epsilon^2)}}+$$
$$\underbrace{\frac{4El_1^2\kappa_1V_{1,23}}{1+v}+\frac{El_1^2(7\kappa_3V_{2,33}-11\kappa_2V_{3,22})}{25}-\frac{14El_1^2(\kappa_2V_{2,23}-\kappa_3V_{3,23})}{25}+\frac{El_1^2(11\kappa_3V_{2,22}-7\kappa_2V_{3,22})}{25}}_{\boldsymbol{O(E\epsilon^2\delta_b)}}+$$
$$\underbrace{\frac{El_1^2\{9({V_{1,33}}^2+{V_{2,33}}^2)+11{V_{3,33}}^2\}}{25(1+v)}+\cdots}_{\boldsymbol{O(E\epsilon^2\delta_b^2)}}+\underbrace{\frac{4El_1^2V_{1,23}(V_{2,13}+V_{3,12})}{1+v}+\cdots}_{\boldsymbol{O(E\epsilon^2\delta_b^3)}}+$$
$$\underbrace{\frac{2El_1^2(18{V_{1,13}}^2+25{V_{2,13}}^2+18{V_{3,13}}^2)}{25(1+v)}+\frac{28El_1^2V_{3,13}V_{2,12}}{25(1+v)}+\cdots}_{\boldsymbol{O(E\epsilon^2\delta_b^4)}}+$$
$$\underbrace{\frac{36El_1^2(V_{1,12}V_{2,11}+V_{1,13}V_{3,11})}{25(1+v)}-\frac{22El_1^2V_{1,11}(V_{3,13}+V_{2,12})}{25(1+v)}}_{\boldsymbol{O(E\epsilon^2\delta_b^5)}}+$$
$$\underbrace{\frac{El_1^2\{11{V_{1,11}}^2+9({V_{2,11}}^2+{V_{3,11}}^2)\}}{25(1+v)}}_{\boldsymbol{O(E\epsilon^2\delta_b^6)}} \tag{63c}$$

$$U^f_{higher3}=\underbrace{\frac{El_2^2\{2\kappa_1^2+(1+v)^2(\kappa_2^2+\kappa_3^2)\}}{2(1+v)}}_{\boldsymbol{O(E\epsilon^2)}}+\underbrace{\frac{El_2^2\{\kappa_2(V_{3,22}-V_{2,23})+\kappa_3(V_{3,23}-V_{2,33})\}}{2}}_{\boldsymbol{O(E\epsilon^2\delta_b)}}+\underbrace{\frac{El_2^2\kappa_1V_{1,23}}{2(1+v)}}_{}+$$
$$\underbrace{\frac{El_2^2({V_{1,33}}^2+{V_{2,33}}^2+2{V_{1,23}}^2+{V_{2,23}}^2)}{8(1+v)}+\cdots}_{\boldsymbol{O(E\epsilon^2\delta_b^2)}}+$$
$$\underbrace{\frac{El_2^2V_{1,13}(V_{3,22}-V_{2,23})}{4(1+v)}+\frac{El_2^2}{2}(\kappa_3V_{2,11}-\kappa_2V_{3,11})+\cdots}_{\boldsymbol{O(E\epsilon^2\delta_b^3)}}+$$

$$\underbrace{\frac{El_2^2(V_{1,12}{}^2+V_{2,12}{}^2+2V_{3,12}{}^2)}{8(1+v)}+\frac{El_2^2(V_{1,13}{}^2+2V_{2,13}{}^2+V_{3,13}{}^2)}{8(1+v)}+\cdots.}_{\boldsymbol{O(E\epsilon^2\delta_b^4)}}-$$
$$\underbrace{\frac{El_2^2(V_{2,11}V_{1,12}+V_{3,11}V_{1,13})}{4(1+v)}}_{\boldsymbol{O(E\epsilon^2\delta_b^5)}}+\underbrace{\frac{El_2^2(V_{2,11}{}^2+V_{3,11}{}^2)}{8(1+v)}}_{\boldsymbol{O(E\epsilon^2\delta_b^6)}} \tag{63d}$$

It is observed that the warping results of the first-order approximation are the same as the zeroth-order solutions. This is also evident for the classical case [43]:

$$\begin{aligned} w_1^f &= x_2\, x_3\, \kappa_1 \\ w_2^f &= \frac{1}{24}v[-24x_2(\gamma_{11}+x_3\kappa_2)+12\,x_2^2\kappa_3+(h^2-b^2-12x_3^2)\kappa_3] \\ w_3^f &= \frac{1}{24}v[(h^2-b^2-12x_2^2)\kappa_2-12\,x_3^2\kappa_2-24x_3(\gamma_{11}-x_2\kappa_3)] \end{aligned} \tag{64}$$

Again, following the same procedure as for the zeroth-order, the 1-D constitutive law for the first-order beam can be written as follows:

$$U_{1Df}=\frac{1}{2}\begin{Bmatrix}\gamma_{11}\\ \kappa_1\\ \kappa_2\\ \kappa_3\end{Bmatrix}^T\begin{bmatrix}Ebh & 0 & 0 & 0\\ 0 & \frac{Ebh(b^2+36l_1^2+9l_2^2)}{3(1+v)} & 0 & 0\\ 0 & 0 & S_{s33f}(l_o,l_1,l_2) & 0\\ 0 & 0 & 0 & S_{s44f}(l_o,l_1,l_2)\end{bmatrix}\begin{Bmatrix}\gamma_{11}\\ \kappa_1\\ \kappa_2\\ \kappa_3\end{Bmatrix} \tag{65}$$

where,

$$\begin{aligned} S_{s33f}(l_o,l_1,l_2) &= \frac{E\,b^3h}{12}+\frac{E\,b\,h\,l_o^2\,(1-8v+12v^2)}{(1+v)}+\frac{18\,E\,b\,h\,l_1^2\,(1+3v)}{25} \\ &\quad +E\,b\,h\,l_2^2\,(1+3v) \\ S_{s44f}(l_o,l_1,l_2) &= \frac{E\,b^3h}{12}+\frac{E\,b\,h\,l_o^2\,(1-8v+12v^2)}{(1+v)}+\frac{18\,E\,b\,h\,l_1^2\,(1+3v)}{25}+E\,b\,h\,l_2^2\,(1+3v) \end{aligned}$$

Here, S_{s33f} and S_{s44f} are the first-order bending stiffness terms. It can be seen that the Poisson's ratio effect enters in this approximation. Additionally, when the length-scale parameters are set to zero, eliminating the strain gradient effects, the first-order stiffness results converge to those obtained using the classical strain energy expression in the VAM derivation. Notably, in the VAM solution without strain gradient theory (i.e., without strain gradient terms), first-order solutions only affect the torsional stiffness, not the bending stiffness. However, in the VAM model that accounts for strain gradient effects, the first-order solutions influence both the bending and torsional stiffnesses. This means that both bending and torsional stiffnesses include additional terms, such as Poisson's effect, beyond what was derived from the zeroth-order approximation. Additionally, it is important to note that at higher orders, the strain gradient effect is significantly more critical than Poisson's ratio effect, highlighting the importance of small-size effects.

4.3. Comparison of results with published literature

From the computed results, it is evident that including the strain gradient effects leads to an increase in the beam bending stiffness. This effect is corroborated in the published literature as well [28-31]. In the work by Zhou et al. [16], the reformulation of the strain gradient elasticity theory was carried out to generate constitutive relations for isotropic material. In their work, they developed higher-order metrics by carrying out further decomposition of the strain gradient tensor into hydrostatic/deviatoric part and

symmetric/antisymmetric part. They studied the bending rigidity, D_z and calculated it as:

$$D_z = E * I + 2\mu A\left[l_o^2(1-2v)^2 + \left(\frac{1}{5}l_o^2 + \frac{4}{15}l_1^2 + l_2^2\right)(1+v)^2\right] \tag{66}$$

The above bending rigidity is normalised using the classical bending rigidity, EI, and following expression is obtained (for square cross section case):

$$\frac{D_z}{EI} = 1 + \frac{12\left[\frac{4}{15}l_1^2(1+v) + l_2^2(1+v) + l_o^2\frac{3(2-6v+7v^2)}{5(1+v)}\right]}{b^2} \tag{67}$$

From the current study, the normalised bending rigidity from the zeroth-order solution, S_{sg} is as follows:

$$\frac{S_{sg}(l_o,l_1,l_2)}{EI} = 1 + \frac{12\left[\frac{18}{25}l_1^2(1+v) + l_2^2(1+v) + l_o^2\frac{(1-2v)^2}{(1+v)}\right]}{b^2} \tag{68}$$

Defining l^* for both the Eq.66. and 67 such that it captures the effective behaviour of the material length-scale parameters in the normalised bending rigidity, the following condensed form can be obtained:

$$\frac{D}{EI} = 1 + \frac{12\,(l^*)^2}{b^2} \tag{69}$$

where, D represents bending rigidity and for Eq.66 $(l^*)^2 = \frac{4}{15}l_1^2(1+v) + l_2^2(1+v) + l_o^2\frac{3(2-6v+7v^2)}{5(1+v)}$ and for Eq 67, $(l^*)^2 = \frac{18}{25}l_1^2(1+v) + l_2^2(1+v) + l_o^2\frac{(1-2v)^2}{(1+v)}$. Here, the three-parameter version as in [16] is taken. It can be seen that by the zeroth-order approximation itself, the bending rigidity terms containing the higher-order length-scale parameters have been effectively captured. Taking the length-scale parameters to be equal i.e., $l_o = l_1 = l_2 = l$, it can be seen that the bending rigidity from current work and from Zhao et al. [16] lie within the 20% difference limit. This is shown in the plot for different Poisson's ratio values in Fig.3. The difference is attributed to the additional warping terms that result from the more accurate VAM procedure which are not present in the beam model presented in the literature.

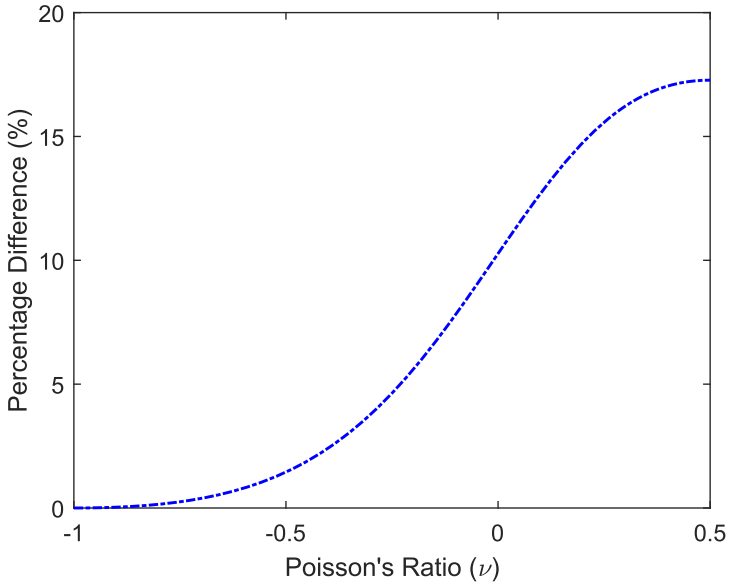

Fig.3. Percentage difference between current model and Zhou et al. [16] for different Poisson's ratio.

As observed in Zhou et al. [16], the current work also shows that all three material length-scale parameters influence the pure bending problem, highlighting the importance of using multiple length-scale parameters to accurately capture small-size effects for bending loads. The normalised bending rigidity is plotted against the beam width to length-scale parameter (h/l^*) ratio, to demonstrate the size dependency of the bending rigidity. In this case, Poisson's effect is ignored i.e., v=0. All length-scale parameters are assumed equal, and the beam width (h) is varied to observe the changes in normalized bending rigidity with respect to beam width. This is as shown in Fig.4.

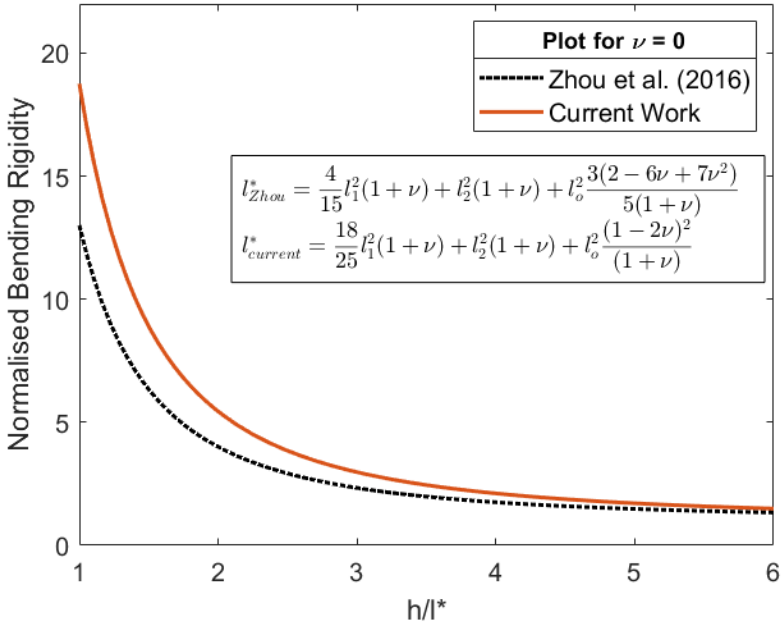

Fig.4. Size effect of normalised bending rigidity

As the h/l^* ratio increases, the normalised bending rigidity decreases in both the current work and the work reported in the literature, demonstrating the accuracy of the current

model. This indicates that small-scale effects become significant when the micro beam thickness is comparable to the material length-scale parameter, with closer values resulting in higher beam stiffness. A slight discrepancy exists between the current work and literature. This may be attributed to the unique warping formulation adopted in the current work, which cannot be found elsewhere in the literature. However, the difference in results with published literature diminishes for higher beam thickness values.

4.4. Numerical Results

This section gives the displacement/deflection results for the strain gradient modified beam. The VAM-derived strain gradient beam model is applied for determining the deflection of micro beams when subjected to bending load. Two different boundary conditions, namely, the cantilever and simply supported are applied.

4.4.1. Cantilever Boundary Condition

Cantilever boundary condition of the example micro beam is considered first, see Fig.5. A transverse vertical concentrated load at the free end of the beam is applied, as shown, to investigate the bending behaviour of the beam, considering the strain gradient effects.

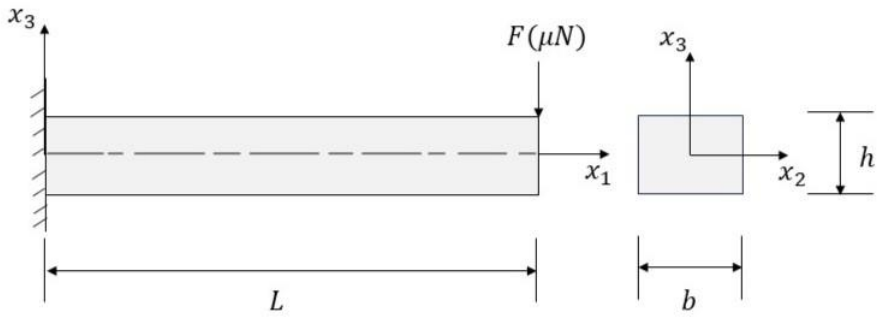

Fig.5. Schematic representation of a cantilever micro beam with concentrated load applied at free end

The micro beam example here, is essentially an epoxy micro beam having the following properties: E=1.44 GPa, v=0.38, l=17.6 μm taken from the literature [25]. Fig.6 shows the bending displacement of the beam along its length for various beam widths and depths. As the beam width decreases, the difference between the classical Euler-Bernoulli results and the proposed VAM strain gradient beam model increases, highlighting the importance of considering higher-order length-scale effects for smaller structures. The results from classical Euler-Bernoulli beam theory, VAM results using classical strain energy expression i.e., without the strain gradient terms (zeroth- and first-order), and the current results incorporating strain gradient theory with higher-order length-scale parameters within VAM framework (zeroth- and first-order) are shown alongside with each other for different beam thicknesses (Fig. 6(a)-(d)). The graphs indicate that for smaller structures, the influence of material length-scale parameters increases, revealing the inaccuracy of classical beam theory for these length scales. As beam thickness increases, the strain gradient results converge to the classical results, demonstrating that classical theory remains valid for larger structures. Therefore, designing micro- and nano-scale structures necessitates the inclusion of material length-scale parameters for

accurate results and the physics depiction of the problem. This paper also presents, for the first time, a higher-order theory incorporating strain gradients i.e. VAM-based first-order approximation for the model including strain gradient terms. It is clear that the VAM strain gradient first-order theory results in even more beam stiffening, as beam deflections are lower than those in the VAM strain gradient zeroth-order model due to the additional Poisson's ratio effect and small-size effects from the material length-scale parameters. For the first-order case, increasing beam thickness leads to deflections converging to those of the classical models, showcasing that size effects are more predominant than the Poisson's ratio effects in micro- and nano-scale structures.

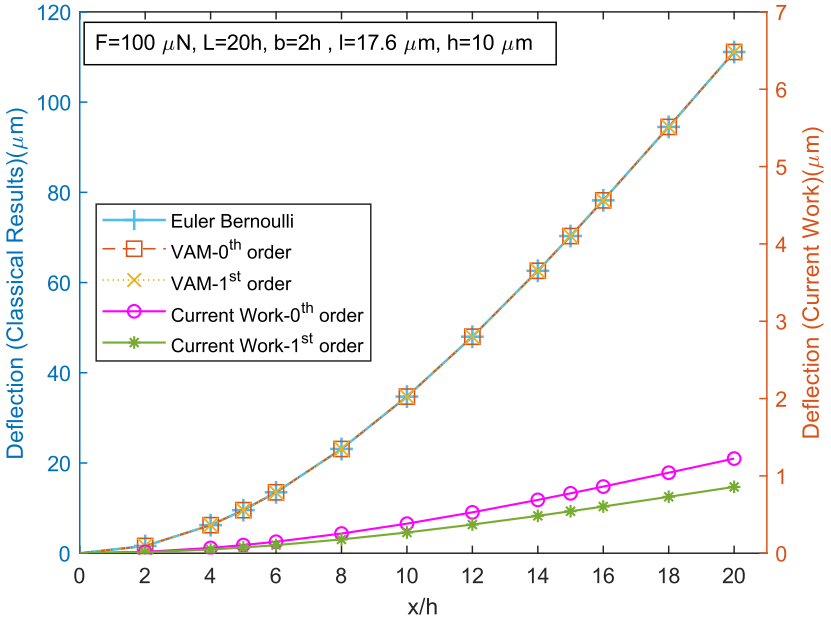

(a)

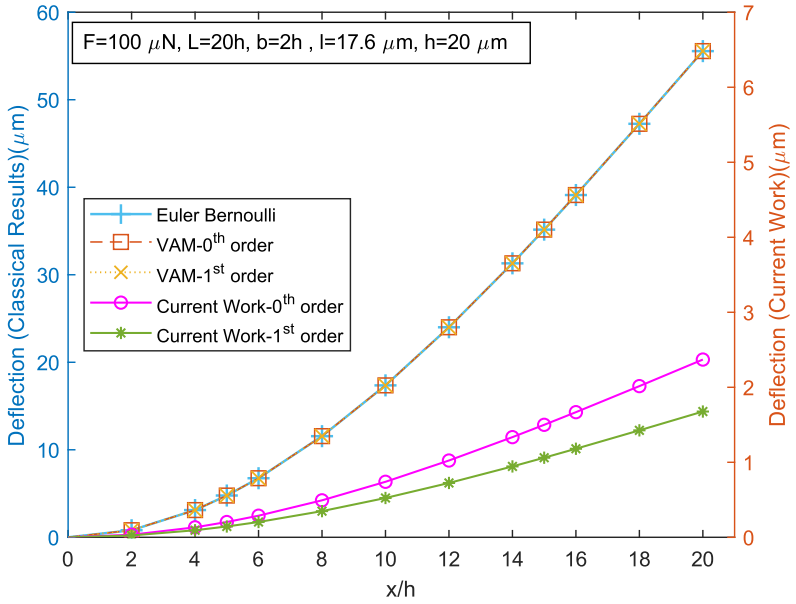

(b)

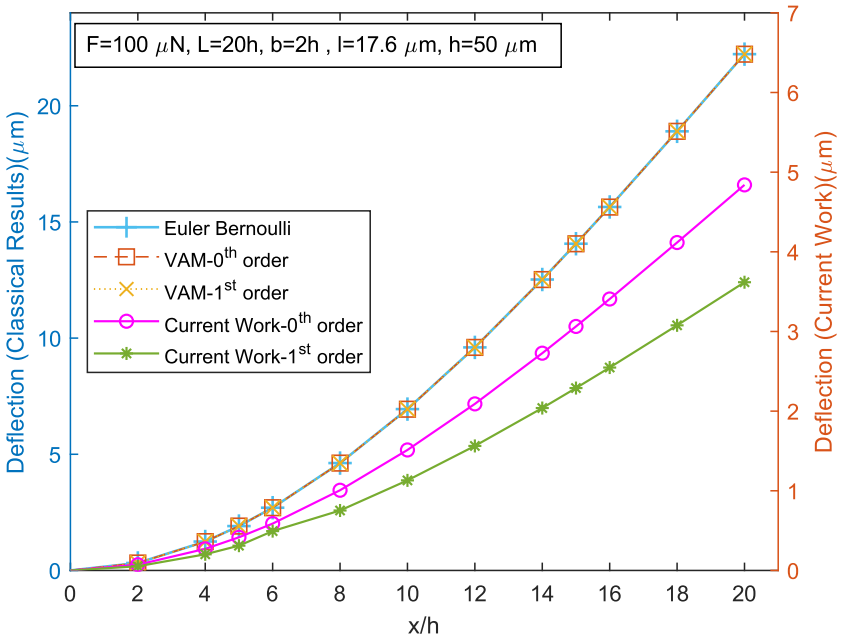

(c)

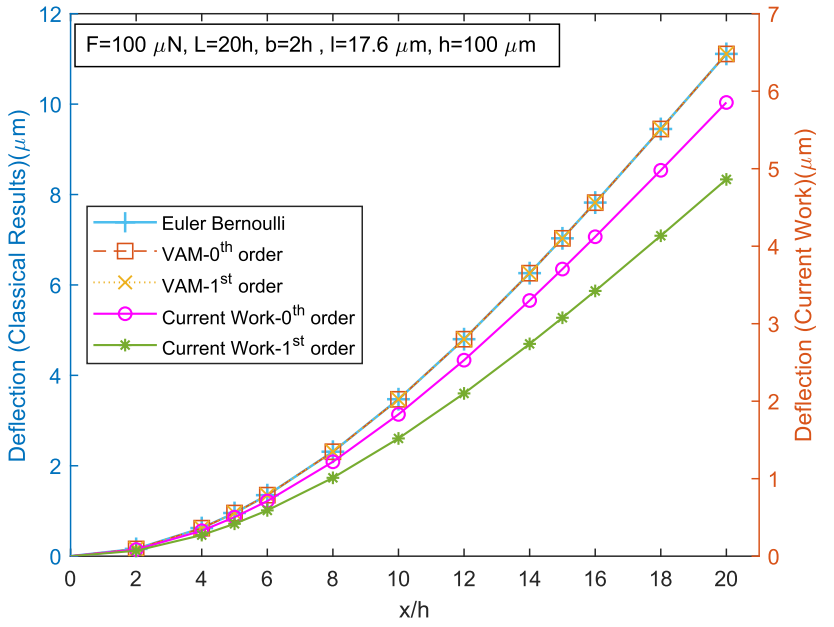

(d)

Fig.6. Comparison of bending deflection of cantilever epoxy micro beam for various beam models for different beam thickness (a) h=10 μm (b) h=20 μm (c) h=50 μm (d) h=100 μm

Next, the special case of a square beam ($b = h$), derived from the rectangular case, is considered. The material properties and other parameters remain unchanged; only the cross-sectional geometry differs. These results are shown in Fig.7. The trend remains consistent with the rectangular case, except that the magnitudes of the deflections change along the length. For square cross sections, the strain gradient VAM models (zeroth- and first-order) also exhibit

stiffening behaviour, with the beams deflecting less than in the classical VAM or Euler-Bernoulli cases. Thus, the small-size effect is effectively captured for different beam thicknesses and cross-sectional shapes under cantilever boundary conditions. This emphasises the necessity of incorporating these effects when modelling micro- and nano-structures, especially when subjected to bending loads.

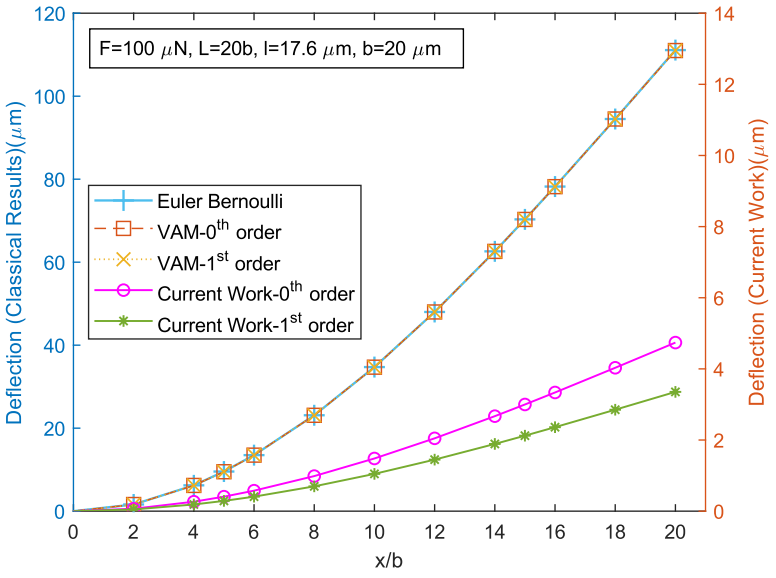

(a)

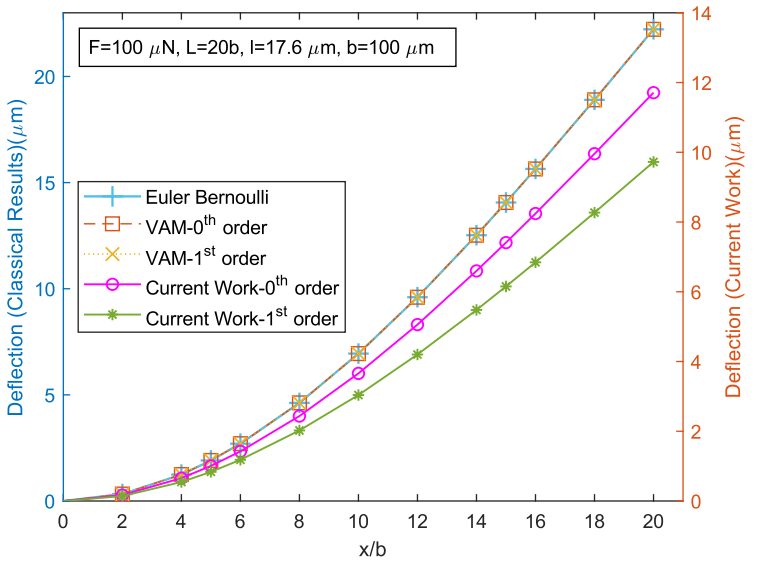

(b)

Fig.7. Comparison of bending deflection of cantilever epoxy micro beam (square cross section) for various beam models for different beam width b (a) b=20 μm (b) b=100 μm

4.4.2. Simply Supported Boundary Condition

For the simply supported boundary condition case, a uniformly distributed transverse bending load is applied to the beam, as shown in Fig.8. All other beam parameters are taken to be the same as the cantilever beam. The

magnitude of the total distributed load applied is 500 μN. Fig.9 shows the bending displacement of the beam for various beam widths and depths.

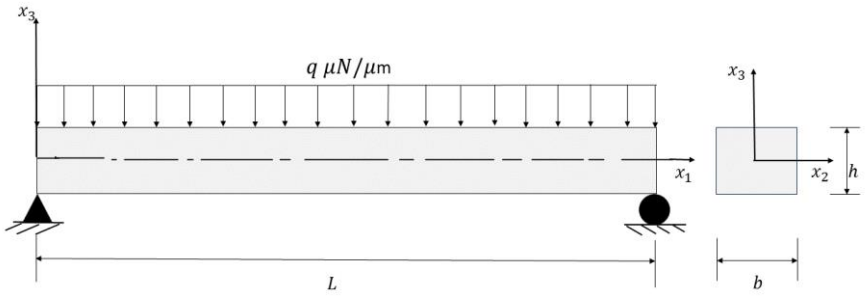

Fig.8. Schematic representation of a simply supported micro beam with uniformly distributed transverse load

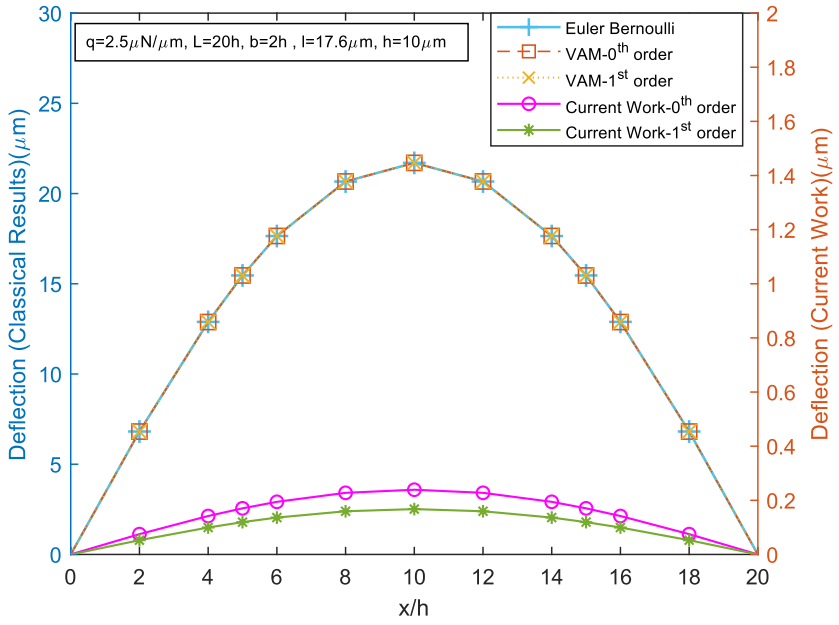

(a)

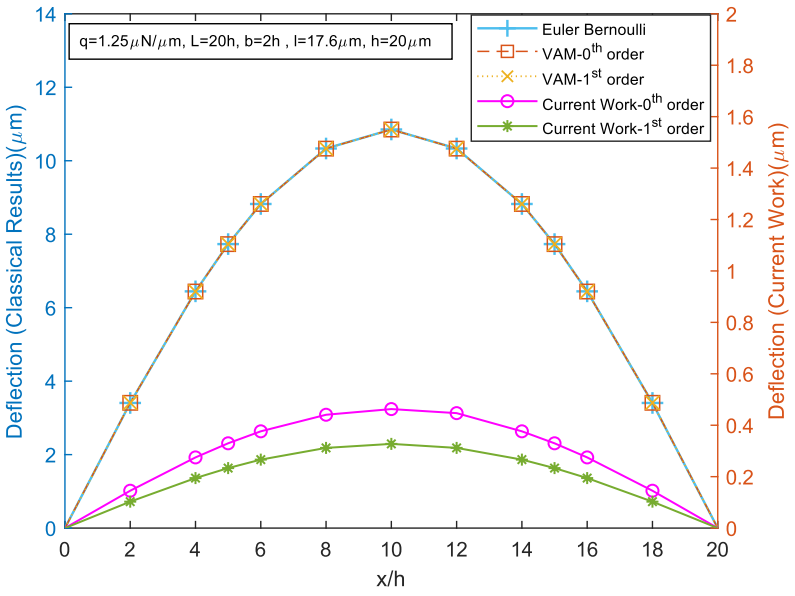
q=1.25μN/μm, L=20h, b=2h , l=17.6μm, h=20μm
Euler Bernoulli
VAM-0th order
VAM-1st order
Current Work-0th order
Current Work-1st order
Deflection (Classical Results)(μm)
Deflection (Current Work)(μm)
x/h

(b)

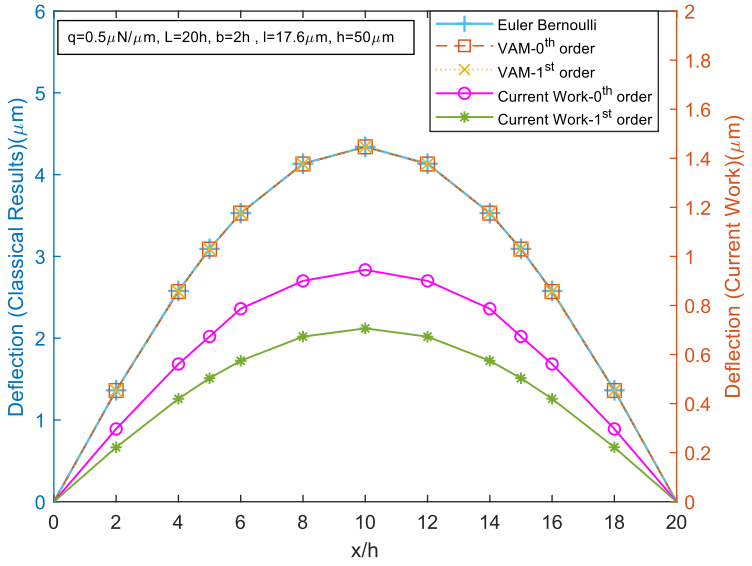
q=0.5μN/μm, L=20h, b=2h , l=17.6μm, h=50μm
Euler Bernoulli
VAM-0th order
VAM-1st order
Current Work-0th order
Current Work-1st order
Deflection (Classical Results)(μm)
Deflection (Current Work)(μm)
x/h

(c)

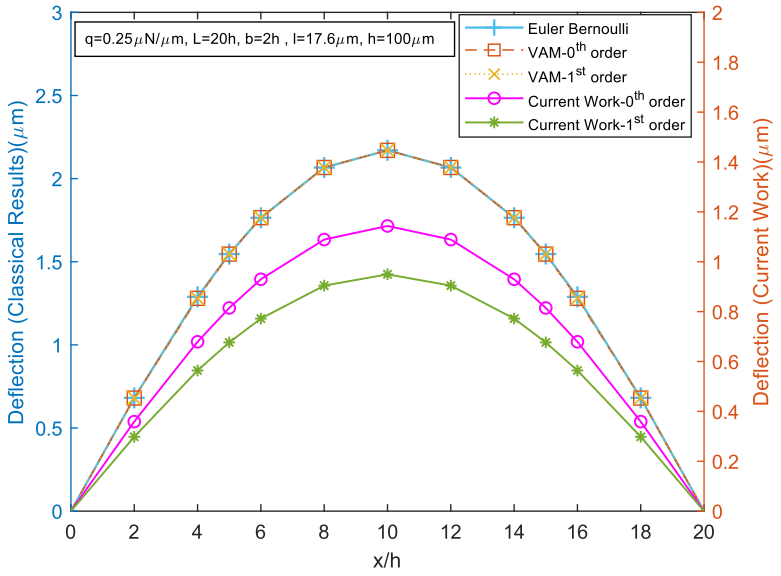

(d)

Fig.9. Comparison of bending deflection of simply supported epoxy micro beam for various beam models for different beam thickness h (a) h=10 μm (b) h=20 μm (c) h=50 μm (d) h=100 μm

Four different beam thickness values (h=10, 20, 50 and 100 μm) have been considered and small-size-effect for simply supported beam boundary condition has been demonstrated. It is clear from Fig. 9.(a)–(d), that for simply supported boundary condition, the non-classical effect dominates the bending behaviour of the beam, showcasing smaller deflections than the classical counterpart for smaller beam thickness, as was the case with cantilever beam. As the thickness value increases from 10 to 100 μm, difference between classical and non-classical deflection results become lesser as the impact of small-size effect diminishes.

Furthermore, taking the case of the square cross section beam, wherein $b = h$, a few other cases for the simply supported boundary conditions were also investigated focusing the analysis on the effect of changing cross sectional length parameter on the bending behaviour. The applied load was a uniformly distributed load (q) of total magnitude 500 μN for all the cases. Two thickness values of 20 and 100 μm were considered. The results are shown in Fig.10. It is clearly seen from the figure that 20 μm shows the maximum difference between classical and non-classical deflections whereas 100 μm gives the least difference between the two cases.

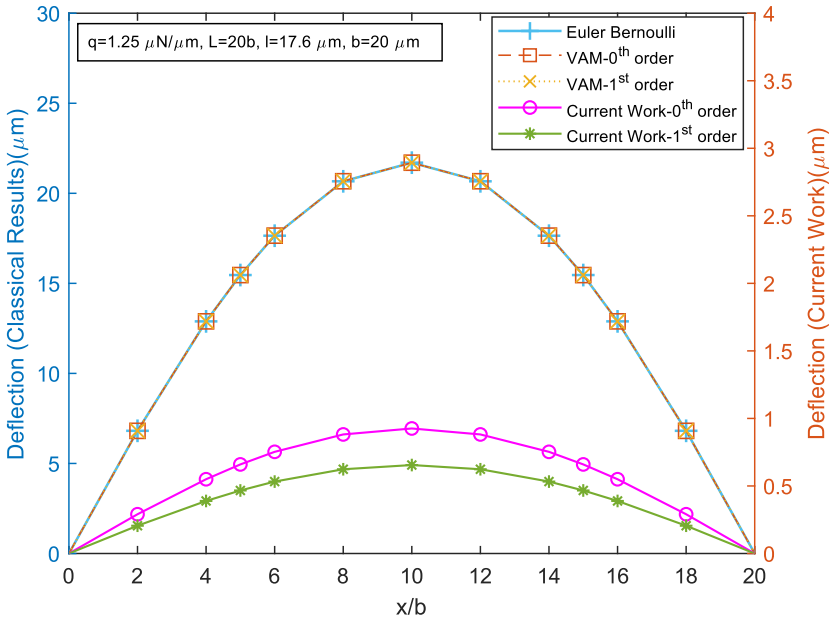

(a)

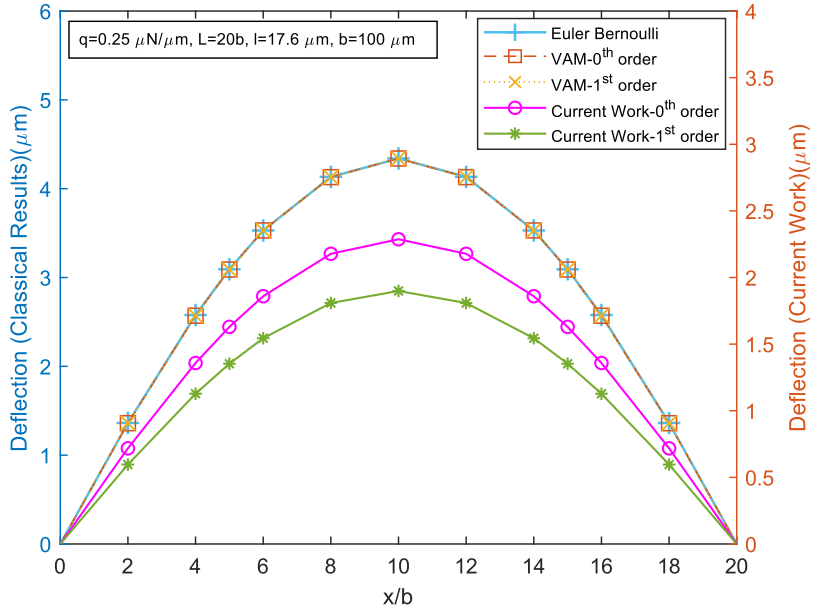

(b)

Fig.10. Comparison of bending deflection of simply supported epoxy micro beam (square cross section) for various beam models for different beam width b (a) b=20 μm (b) b=100 μm

The results clearly show that cross-sectional dimensions significantly influence the importance of considering small-scale parameters. As the beam size increases, the difference between classical results and the higher-order VAM-based models proposed in this work diminishes, as expected. The small-size effect is demonstrated for two different beam boundary conditions and two cross section types (rectangular and square). However, this effect primarily depends on the beam thickness and material length-scale parameter, with the difference being more pronounced when these values are similar. Therefore, for

bending load cases, it is crucial to include the small-size effects described by the strain gradient theory to accurately model and predict the behaviour of micro- and nano-scale structures.

4.5. Application to Carbon Nano Tube (CNT) reinforced composite micro beam

In this section, the behaviour of the CNT-based nanocomposite beam when subjected to bending loads is modelled. It is widely known that the non-classical effects must be captured to model nanocomposites in a continuum framework. The higher-order gradient effect using the derived beam model for the CNT-reinforced nanocomposite is considered here. For a micro beam of uniformly distributed CNT-based nanocomposite, the homogenised nanocomposite properties are estimated using the simple Voigt's homogenisation rule of mixtures as follows:

$$E_{eq} = E_{CNT}\mathrm{v}_{CNT} + E_m(1 - \mathrm{v}_{CNT}) \tag{70}$$

$$v_{eq} = v_{CNT}\mathrm{v}_{CNT} + v_m(1 - \mathrm{v}_{CNT}) \tag{71}$$

where, E_{eq} is the equivalent elastic modulus of the nanocomposites, E_{CNT} is the elastic modulus of the CNT, E_m is the elastic modulus of the matrix, v_{eq} is the equivalent Poisson's ratio of the nanocomposite, v_m & v_{CNT} are the Poisson's ratio of CNT and matrix respectively and v_{CNT} is the volume fraction of the CNT in the nanocomposite. The CNT volume fraction for uniform distribution case is estimated as follows [60]:

$$\mathrm{v}_{CNT} = \frac{m_{CNT}}{m_{CNT} + \frac{\rho_{CNT}}{\rho_m} - \frac{\rho_{CNT}}{\rho_m} m_{CNT}} \tag{72}$$

Here, m_{CNT} is the mass fraction of CNT, ρ_{CNT} is the density of CNT and ρ_m is the density of the matrix. The parameters taken are as follows: E_{CNT}= 899.7 GPa, v_{CNT} = 0.19, $v_m = 0.38$, $E_m = 2.5$ GPa, ρ_{CNT} =1400 kg/m^3, ρ_m=1190 kg/m^3 [60]. Also, the dimensions of the CNT-reinforced nanocomposite micro beam are- $L = 100$ μm, b=3.5 μm, h=5 μm. The variation of the bending deflection for a cantilever boundary condition case for different values of length-scale parameter varying from 0 to h at different locations 'x' along the beam length is studied. The results are shown in Fig.11. As the length-scale parameter is increased, stiffening of the nanocomposite beam occurs. The interplay between the CNT content (volume fraction) and the small-size effect is successfully demonstrated here by showcasing deflections at each point along the beam length and for different values of the material length-scale parameter. For higher CNT volume fraction, this stiffening effect is enhanced further. These results are obtained using the first-order approximation of the strain gradient theory-based VAM formulation for rectangular beams.

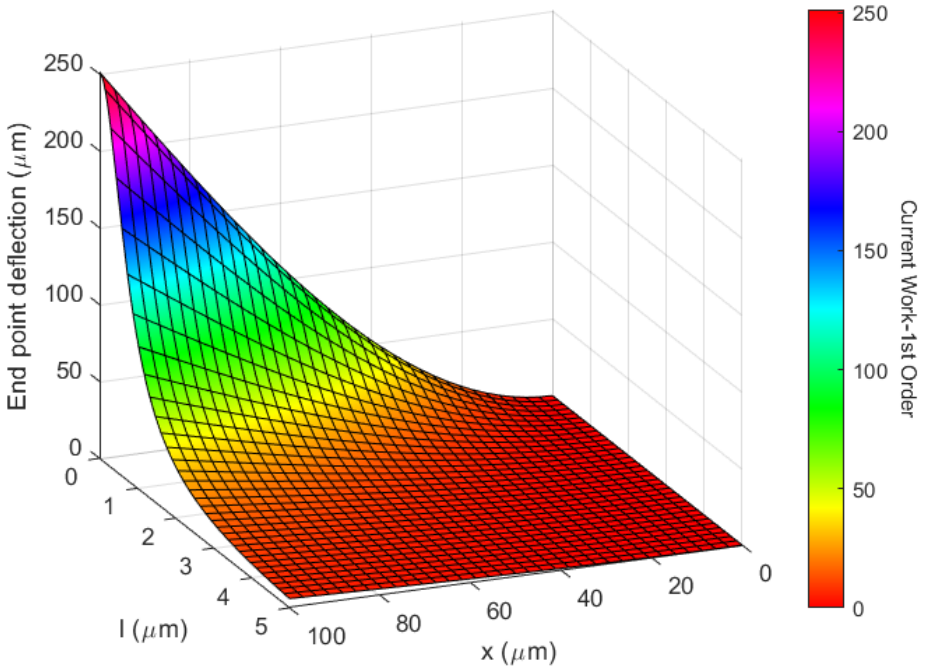
End point deflection (μm)
250
200
150
100
50
0
0
1
2
3
4
5
l (μm)
100
80
60
40
20
0
x (μm)
Current Work-1st Order
250
200
150
100
50
0

(a)

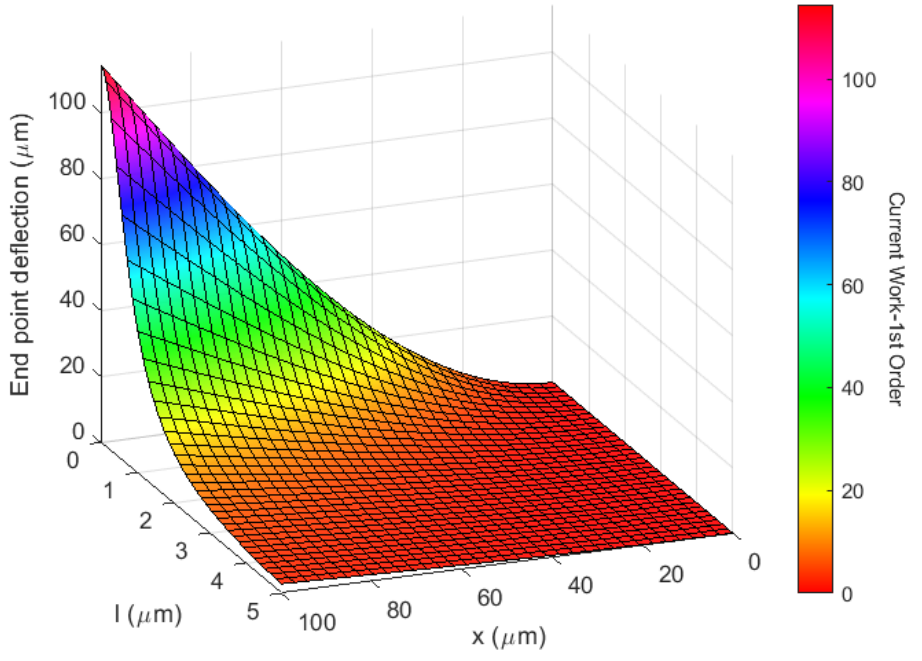
End point deflection (μm)
100
80
60
40
20
0
0
1
2
3
4
5
l (μm)
100
80
60
40
20
0
x (μm)
Current Work-1st Order
100
80
60
40
20
0

(b)

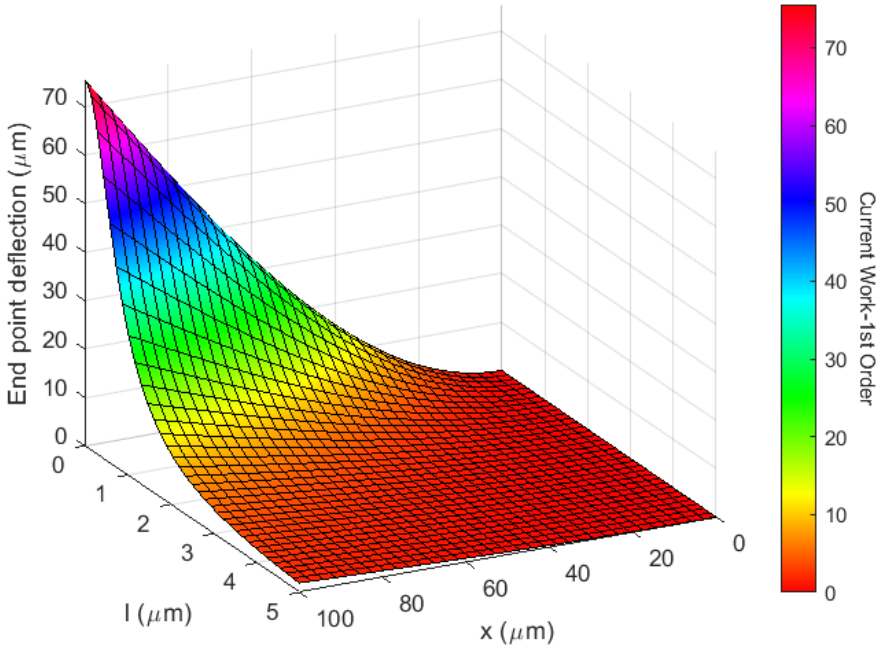

(c)

Fig.11. Bending deflection of cantilever CNT composite micro beam (Rectangular cross section) for various beam models with different beam CNT volume fraction (a) v_{CNT}=0.078 (b) v_{CNT} =0.175 (c) v_{CNT} = 0.267

It can be seen from the above results that for the classical case, which is when l is 0, the CNT composite nano beam has the maximum deflection. Further, upon increasing the length-scale parameters, the end deflection reduces and is minimum for the case when $l = h$. The volume fractions of CNT have been taken considering practically reachable limits in mind. Thus, showcasing the importance of modelling the small-size effect of CNT-based nanocomposite structures. The huge difference between classical and current results emphasises this point even more strongly.

5. Conclusions and future directions

This paper presents a novel beam model that integrates modified strain gradient theory into the Variational Asymptotic Method (VAM) to capture non-classical strain gradient effects influenced by material length-scale parameters. The analysis investigates three distinct length-scale cases: $O(l) \ll O(b)$, $O(l) = O(L)$) and $O(l) = O(b)$, where l is the material length-scale parameter and b is the width of the beam. The investigation has identified the critical point at which these parameters significantly affect the mechanical behaviour of micro/nano beams. By employing zeroth- and first-order asymptotic approximations, the study highlights the importance of small-size effects, even for higher-order beam model approximations, which have not been previously explored within the VAM framework. Comparisons with existing literature show good agreement, with observed differences which can be attributed to more realistic warping solutions introduced in this model.

The application of this modified theory to composite micro beams reinforced with CNTs reveals a notable stiffening effect, underscoring the limitations of classical elastic models in describing micro- and nano-scale beam mechanics. Although the current focus is on beams with rectangular and square cross-sections, future work will extend the approach to nanostructures like graphene sheets and carbon nanotubes, where size effects and geometric

nonlinearity play crucial roles. Notably, for thin structures undergoing large displacements and rotations, nonlinear geometric behaviours become significant for which the presented approach sets the stage for a deeper understanding of the intricate mechanics of micro and nano-scale structures.

Future research will explore non-classical boundary conditions and develop numerical solutions to the boundary value problems identified, addressing the limitations of current strain gradient models. These efforts will further refine our understanding of the behaviour of micro and nano structures under various boundary conditions, advancing the study of small-scale beam mechanics. Additionally, other non-classical approaches, such as nonlocal theories, granular micromechanics, and higher-order continuum models, will be investigated within the VAM framework to expand its applicability and enhance its capability in modelling small-scale effects.

6. References

[1] Thai HT, Vo TP, Nguyen TK, Kim SE. A review of continuum mechanics models for size-dependent analysis of beams and plates. Compos Struct 2017; 177: 196–219.

[2] Roudbari MA, Jorshari TD, Lü C, Ansari R, Kouzani AZ, Amabili M. A review of size-dependent continuum mechanics models for micro- and nano-structures. Thin-Walled Struct 2022; 170: 108562.

[3] Zhao J, Zhou S, Wang B, Wang X. Nonlinear microbeam model based on strain gradient theory. Appl Math Model 2012; 36: 2674–2686.

[4] Li C, Yao L, Chen W, Li S. Comments on nonlocal effects in nano-cantilever beams. Int J Eng Sci 2015; 87: 47–57.

[5] Liang X, Hu S, Shen S. A new Bernoulli–Euler beam model based on a simplified strain gradient elasticity theory and its applications. Compos Struct 2014; 111: 317–323.

[6] Miandoab EM, Yousefi-Koma A, Pishkenari HN. Poly silicon nanobeam model based on strain gradient theory. Mech Res Commun 2014; 62: 83–88.

[7] Sidhardh S, Ray MC. Exact solutions for elastic response in micro- and nano-beams considering strain gradient elasticity. Math Mech Solids 2019; 24(4): 895–918.

[8] Khaje khabaz M, Eftekhari SA, Toghraie D. Vibration and dynamic analysis of a cantilever sandwich microbeam integrated with piezoelectric layers based on strain gradient theory and surface effects. Appl Math Comput 2022; 419: 126867.

[9] Nazarenko L, Gluge R, Altenbach H. On variational principles in coupled strain-gradient elasticity. Math Mech Solids 2022; 27(10): 2256–2274.

[10] Mindlin RD. Micro-structure in linear elasticity. Arch Ration Mech Anal 1964; 16: 51–78.

[11] Toupin RA. Elastic materials with couple-stresses. Arch Ration Mech Anal 1962; 11: 385–414.

[12] Koiter WT. Couple-stresses in the theory of elasticity: I and II. Proceedings of the Koninklijke Nederlandse Akademievan Wetenschappen 1964; 67: 17–44.

[13] Yang F, Chong ACM, Lam DCC, Tong P. Couple stress based strain gradient theory for elasticity. Int J Solids Struct 2002; 39(10): 2731–2743.

[14] Lam DCC, Yang F, Chong ACM, Wang J, Tong P. Experiments and theory in strain gradient elasticity. J Mech Phys Solids 2003; 51: 1477–1508.

[15] Mindlin RD, Eshel NN. On first strain-gradient theories in linear elasticity. Int J Solids Struct 1968; 4: 109–124.

[16] Zhou S, Li A, Wang B. A reformulation of constitutive relations in the strain gradient elasticity theory for isotropic materials. Int J Solids Struct 2016; 80: 28–37.

[17] Khorshidi MA. The material length scale parameter used in couple stress theories is not a material constant. Int J Eng Sci 2018; 133: 15–25.

[18] Yaghoubi ST, Balobanov V, Mousavi SM, Niiranen J. Variational formulations and isogeometric analysis for the dynamics of anisotropic gradient-elastic Euler-Bernoulli and shear-deformable beams. Eur J Mech A Solids 2020; 69: 113–123.
[19] Zhang G, Gao XL. A new Bernoulli–Euler beam model based on a reformulated strain gradient elasticity theory. Math Mech Solids 2020; 25(3): 630–643.
[20] Barretta R, Faghidian SA, Marotti de Sciarra F, Vaccaro MS. Nonlocal strain gradient torsion of elastic beams: variational formulation and constitutive boundary conditions. Arch Appl Mech 2020; 90: 691–706.
[21] Vo D, Aung ZY, Le TM, Suttakul P, Atroschenko E, Rungamornrat J. Analysis of planar arbitrarily curved microbeams with simplified strain gradient theory and Timoshenko–Ehrenfest beam model. Math Mech Solids 2024; 29(9): 1787–1828.
[22] Liang X, Hu S, Shen S. Bernoulli–Euler dielectric beam model based on strain-gradient effect. J Appl Mech 2013; 80(4): 044502.
[23] Qi L, Zhou S. A size-dependent spherical microshell model based on strain gradient elasticity theory. Eur J Mech A Solids 2020; 84: 104087.
[24] Lu Q, Guangyang F, Shenjie Z. A flexoelectric spherical microshell model incorporating the strain gradient effect. Appl Math Model 2019; 75: 692–708.
[25] Kong S, Zhou S, Nie Z, Wang K. Static and dynamic analysis of micro beams based on strain gradient elasticity theory. Int J Eng Sci 2009; 47: 487–498.
[26] Li A, Wang Q, Song M, Chen J, Su W, Zhou S, et al. On strain gradient theory and its application in bending of beam. Coatings 2022; 12: 1304.
[27] Ashoori A, Mahmoodi MJ. The modified version of strain gradient and couple stress theories in general curvilinear coordinates. Eur J Mech A Solids 2015; 49: 441–454.
[28] Akgöz B, Civalek Ö. Strain gradient elasticity and modified couple stress models for buckling analysis of axially loaded micro-scaled beams. Int J Eng Sci 2011; 49: 1268–1280.
[29] Zhang B, He Y, Liu D, Gan Z, Shen L. Non-classical Timoshenko beam element based on the strain gradient elasticity theory. Finite Elem Anal Des 2014; 79: 22–39.
[30] Asghari M, Kahrobaiyan MH, Nikfar M, Ahmadian MT. A size-dependent nonlinear Timoshenko microbeam model based on the strain gradient theory. Acta Mech 2012; 223: 1223–1249.
[31] Kahrobaiyan MH, Asghari M, Ahmadian MT. Strain gradient beam element. Finite Elem Anal Des 2013; 68: 63–75.
[32] Amiot F. Constitutively optimal governing equations for higher-grade elastic beams. Eur J Mech A Solids 2021; 86: 104195.
[33] Lazopoulos KA, Lazopoulos AK. Bending and buckling of thin strain gradient elastic beam. Eur J Mech A Solids 2010; 29: 837–843.
[34] Dell'isola F, Misra A. Principle of virtual work as foundational framework for metamaterial discovery and rational design. Comptes Rendus. Mécanique 351.S3 2023: 1-25.
[35] Aminpour H, Rizzi N. On the modelling of carbon nano tubes as generalized continua." Generalized continua as models for classical and advanced materials. Cham: Springer International Publishing, 2016. 15-35.
[36] Aminpour H, Rizzi N. A 1D continuum with microstructure for single-wall CNTs bifurcation analysis. Math Mech Solids 2015; 114
[37] Barchiesi, E., Misra, A., Placidi, L., & Turco, E. (2021). Granular micromechanics-based identification of isotropic strain gradient parameters for elastic geometrically nonlinear deformations. ZAMM-Journal of Applied Mathematics and Mechanics/Zeitschrift für Angewandte Mathematik und Mechanik, 101(11)
[38] Misra, A., Placidi, L., dell'Isola, F., & Barchiesi, E. (2021). Identification of a geometrically nonlinear micromorphic continuum via granular micromechanics. Zeitschrift für angewandte Mathematik und Physik, 72, 1-21.

[39] Placidi, L., Barchiesi, E., Dell'Isola, F., Maksimov, V., Misra, A., Rezaei, N., ... & Timofeev, D. (2022). On a hemi-variational formulation for a 2D elasto-plastic-damage strain gradient solid with granular microstructure. Mathematics in Engineering, 5, 1-24.
[40] Placidi, L., Dell'Isola, F., Kandalaft, A., Luciano, R., Majorana, C., & Misra, A. (2024). A granular micromechanic-based model for ultra high performance fiber-reinforced concrete (uhp frc). International Journal of Solids and Structures, 297, 112844.
[41] Riesselmann, J., Rezaei, N., Placidi, L., & Balzani, D. (2024). An efficient mixed finite element formulation for 3D strain gradient elasticity. Computer Methods in Applied Mechanics and Engineering, 432, 117422.
[42] Mindlin R. Second gradient of strain and surface-tension in linear elasticity. Int J Solids Struct 1965; 1(4): 417–438.
[43] Yu W, Hodges DH. Elasticity solutions versus asymptotic sectional analysis of homogeneous, isotropic, prismatic beams. J Appl Mech 2004; 71(1): 15–23.
[44] Hodges DH. Nonlinear composite beam theory. Progress Astronaut Aeronaut 2006; 213: 304.
[45] Sachdeva C, Gupta M, Hodges DH. Modelling of initially curved and twisted smart beams using intrinsic equations. Int J Solids Struct 2018; 148–149: 3–13.
[46] Yu W, Hodges DH, Ho JC. Variational asymptotic beam sectional analysis – an updated version. Int J Eng Sci 2012; 59: 40–64.
[47] Berdichevskii VL. Variational-asymptotic method of constructing a theory of shells: PMM vol. 43, no.4, 1979, pp. 664–687. J Appl Math Mech 1979; 43(4): 711–736.
[48] Volovoi VV, Hodges DH. Theory of anisotropic thin-walled beams. J Appl Mech 2000; 67(3): 453–459.
[49] Rajabi F, Ramezani S. A nonlinear microbeam model based on strain gradient elasticity theory. Acta Mech Solida Sinica 2013; 26(1): 21–34.
[50] Jirásek M, Rolshoven S. Localization properties of strain-softening gradient plasticity models. Part I: Strain-gradient theories. Int J Solids Struct 2009; 46: 2225–2238.
[51] Polizzotto C. Variational formulations and extra boundary conditions within stress gradient elasticity theory with extensions to beam and plate models. Int J Solids Struct 2016; 80: 405–419.
[52] Barretta R, Faghidian SA, Marotti de Sciarra F. Aifantis versus Lam strain gradient models of Bishop elastic rods. Acta Mech 2019; 230: 2799–2812.
[53] Minh Le T, Vo D, Rungamornrat J, Quoc Bui T. Strain-gradient theory for shear deformation free-form microshells: Governing equations of motion and general boundary conditions. Int J Solids Struct 2022; 248: 111579.
[54] Jafari A, Ezzati M. Investigating the non-classical boundary conditions relevant to strain gradient theories. Physica E 2017; 86: 88–102.
[55] Zhu X, Li L. Closed form solution for a nonlocal strain gradient rod in tension. Int J Eng Sci 2017; 119: 16–28.
[56] Polizzotto C. A unifying variational framework for stress gradient and strain gradient elasticity theories. Eur J Mech A Solids 2015; 49: 430–440.
[57] Polizzotto C. Gradient elasticity and nonstandard boundary conditions. Int J Solids Struct 2003; 40: 7399–7423.
[58] Shokrieh MM, Zibaei I. Determination of the appropriate gradient elasticity theory for bending analysis of nano-beams by considering boundary conditions effect. Lat Am J Solids Struct 2015; 12: 2208–2230.
[59] Tang H, Li L, Hu Y, Meng W, Duan K. Vibration of nonlocal strain gradient beams incorporating Poisson's ratio and thickness effects. Thin-Walled Struct 2019; 137: 377–391.
[60] Vaccaro M. On geometrically nonlinear mechanics of nanocomposite beams. Int J Eng Sci 2022; 173: 103653.